| Volumen 42 | Number 1 | **JANUARY-APRIL 2021**

ib

UNA PUBLICACIÓN DE LA
SOMIB
Sociedad Mexicana de Ingeniería Biomédica

Revista Mexicana de Ingeniería Biomédica

Special issue COVID-19

Biomedical Engineering Innovations for Coronavirus

http://www.rmib.mx

ISSN 2395-9126

SOMIB
Sociedad Mexicana de Ingeniería Biomédica

Sociedad Mexicana de Ingeniería Biomédica

La Mesa Directiva de la Sociedad Mexicana de Ingeniería Biomédica hace una extensa invitación a las personas interesadas en participar, colaborar y pertenecer como Socio Activo de la SOMIB. La SOMIB reúne a profesionistas que se desarrollan en áreas de Ingeniería Biomédica, principalmente ingenieros biomédicos, así como otros profesionistas afines con el desarrollo de tecnología para la salud.

Membresía Estudiante
$850.00 ***PESOS MXN***
15% de descuento para grupos de 5 o más personas.

Membresía Profesional
$1,450.00 ***PESOS MXN***
15% de descuento para grupos de 5 o más personas.

Membresía Institucional
$11,600.00 ***PESOS MXN***
No aplica descuento.

Membresía Empresarial
$20,000.00 ***PESOS MXN***
La suscripción empresarial requiere invitación.

EL PAGO CUBRE UN AÑO DE CUOTA. EN CASO DE REQUERIR FACTURA
FAVOR DE SOLICITARLA, ADJUNTANDO COMPROBANTE DE PAGO Y ESPECIFICANDO CONCEPTO,
AL CORREO ELECTRÓNICO: ***facturación@somib.org.mx***

REVISTA MEXICANA DE Ingeniería Biomédica

AUTORES

Los trabajos a publicar en la RMIB, deben ser originales, inéditos y de excelencia. Los costos de publicación para autores son los siguientes:

NO SOCIOS:	***$4,060.00*** ***PESOS MXN*** *(INCLUYE I.V.A.)*
SOCIOS:	***$1,276.00*** ***PESOS MXN*** *(INCLUYE I.V.A.)*

PUBLICIDAD

A las empresas e instituciones interesadas en publicitar su marca o productos en la RMIB, los costos por número son los siguientes:

MEDIA PLANA:	***$4,999.00*** ***PESOS MXN*** *(INCLUYE I.V.A.)*
UNA PLANA:	***$6,799.00*** ***PESOS MXN*** *(INCLUYE I.V.A.)*
CONTRAPORTADA:	***$7,799.00*** ***PESOS MXN*** *(INCLUYE I.V.A.)*
FORROS INTERIORES:	***$7,799.00*** ***PESOS MXN*** *(INCLUYE I.V.A.)*

DESCUENTO DEL **20%** AL CONTRATAR PUBLICIDAD EN DOS O MÁS NÚMEROS.

Para ser socio

- Realiza el pago de derechos, de acuerdo a la categoría que te corresponde.
- Ingresa a *www.somib.org.mx/membresia* y elige el tipo de membresía por el cual realizaste el pago de derechos.
- Completa el formulario correspondiente y envíalo.
- Se emitirá carta de aceptación y número de socio por parte de la mesa directiva (aprobada la solicitud).
- Para mayor información sobre beneficios, ingresar a: *www.somib.org.mx* o comunícate al correo *socios@somib.org.mx*.

Datos bancarios

- **Beneficiario:** *Sociedad Mexicana de Ingeniería Biomédica A. C.*
- **Banco:** *Scotiabank*
- **Referencia:** *1000000333*
- **Cuenta:** *11006665861*
- **CLABE Interbancaria:** *044770110066658614*

La inserción de la publicidad será publicada en el libro electrónico y en el área de patrocinios en el sitio Web de la revista (RMIB), disponible en:

http://rmib.mx

REVISTA MEXICANA DE
Ingeniería Biomédica

Índices
La Revista Mexicana de Ingeniería Biomédica aparece en los siguientes índices científicos:
Sistema de Clasificación de Revistas Científicas y Tecnologías del CONACYT - Q4, SCOPUS, SciELO, EBSCO, Medigraphic Literatura Biomédica, Sociedad Iberoamericana de Información Científica - SIIC.

www.rmib.mx
ISSN 2395-9126

Asistente Editorial
Carla Ivonne Guerrero Robles

Editor Técnico y en Internet
Enrique Ban Sánchez

SOMIB
Sociedad Mexicana de Ingeniería Biomédica

Sociedad Mexicana de Ingeniería Biomédica
Periferico Sur #5374, Col. Olímpica, Alc. Coyoacán, C. P. 04710, Ciudad de México, CDMX, México (555) 574-4505

SOMIB
Sociedad Mexicana de Ingeniería Biomédica

Afiliada a:
International Federation of Medical and Biological Engineering (IFMB-IUPSM-ICSU)
Federación de Sociedades Científicas de México, A.C. (FESOCIME)
Consejo Regional de Ingeniería Biomédica para América Latina (CORAL)

SOMIB
Periferico Sur #5374, Col. Olímpica, Alc. Coyoacán, C. P. 04710, Ciudad de México, CDMX, México (555) 574-4505
www.somib.org.mx

REVISTA MEXICANA DE INGENIERÍA BIOMÉDICA, Vol. 42, No. 1, Enero-Abril 2021, es una publicación cuatrimestral editada por la Sociedad Mexicana de Ingeniería Biomédica A.C., Periferico Sur #5374, Col. Olímpica, Alc. Coyoacán, C. P. 04710, (555) 574-4505, www.somib.org.mx, rmib.somib@gmail.com. Editor responsable: César Antonio Díaz González. Reserva de Derechos al Uso Exclusivo No. 04-2015-041310063800-203, ISSN (impreso) 0188-9532; ISSN (electrónico) 2395-9126, ambos otorgados por el Instituto Nacional del Derecho de Autor. Responsable de la última actualización de este número: Lic. Enrique Federico Ban Sánchez, Periferico Sur #5374, Col. Olímpica, Alc. Coyoacán, C. P. 04710, (555) 574-4505, fecha de última modificación, 1 de agosto de 2020.

Disponible en línea:
www.rmib.mx

CONTENTS
CONTENIDO

LETTER TO EDITOR

Vol. 42 | No. 1 | **JANUARY - APRIL 2021** | pp 6-9

REVISTA MEXICANA DE Ingeniería Biomédica

dx.doi.org/10.17488/RMIB.42.1.1

E-LOCATION ID: 1109

Saliva analysis using FTIR spectroscopy to detect possible SARS-CoV-2 (COVID-19) virus carriers

Miguel Sánchez Brito[1], *Mónica Maribel Mata Miranda*[2], *Adriana Martínez Cuazitl*[3], *Dante J. López Mezquita*[3], *Melissa Guerrero Ruiz*[2], *Gustavo J. Vázquez Zapién*[2]

[1]TecNM/Instituto Tecnológico de Aguascalientes

[2]Escuela Militar de Medicina, Centro Militar de Ciencias de la Salud, Secretaría de la Defensa Nacional

[3]Hospital Central Militar, Secretaría de la Defensa Nacional

Corresponding author

TO: **Gustavo J. Vázquez Zapién**

INSTITUTION: **Escuela Militar de Medicina, Centro Militar de Ciencias de la Salud, Secretaría de la Defensa**

ADDRESS: **Cerrada de Palomas S/N, esquina Periférico, Col. Lomas de San Isidro, C. P. 11200, Alc. Miguel Hidalgo, CDMX, México**

E-MAIL: **gus1202@hotmail.com**

Received:

13 August 2020

Accepted:

9 September 2020

Dear Editor,

The use of saliva in the diagnosis of COVID-19 using the Reverse Transcription Polymerase Chain Reaction (RT-PCR) technique has been implemented largely because it is a minimally invasive technique despite the approximate percentage of accuracy that it allows obtaining (72%) [1] [2]. The Fourier transform infrared spectroscopy (FTIR) is a technique that allows analyzing the molecular structure of a sample through a signal or FTIR spectrum produced by the vibrations of the chemical bonds that make up said sample when impacted by frequencies belonging to infrared radiation [3]. By producing molecular changes [4] [5], viral infections are potentially identifiable by FTIR spectroscopy, so this technique can be advantageous to perform examinations in a more agile way than RT-PCR (72 hours on average) [6] since the spectrum capture takes approximately 15 minutes including the drying time of the sample. Conducting timely tests to identify and isolate infected people is the most efficient methodology as there is no treatment or vaccine against the virus.

Through different regions of the FTIR spectrum, it has been possible to detect characteristic changes of different types of cancer, Parkinson's disease, and diabetes, among other diseases [7] [9], however, related to viral infections, Supti R, *et al*., and Eyal A, *et al*. [10] [11], indicate that viral infections mainly affect the protein region, specifically the region attributed to amide I (1700-1600 cm^{-1}). Spectral changes are reflected by the growth or decrease in a region of the FTIR spectrum, so transforming the spectrum, Figure 1a, through the use of derivatives, Figure 1b, helps to highlight such changes as in the work of Supti R, *et al*., [10].

Despite the advantages above, it is necessary to consider the following challenges presented by saliva analysis using FTIR spectroscopy: excess water, mixing of bonds of different components, and variations

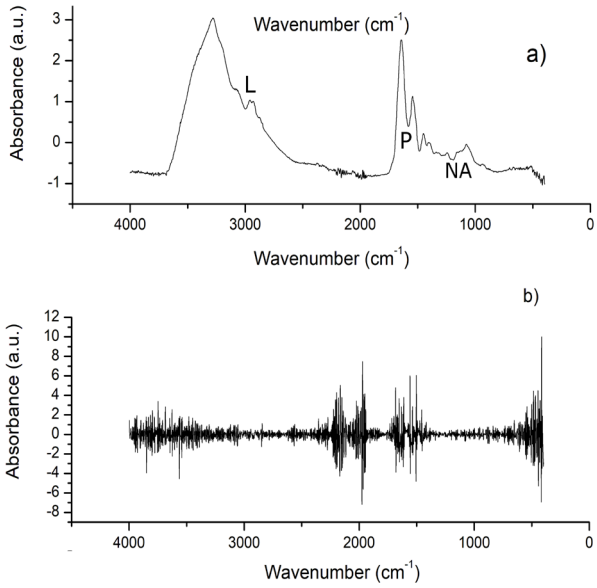

FIGURE 1. a) Main macromolecules of the saliva spectrum, L: Lipids (3000-2800 cm-1), P: Proteins (Amide I and Amida II, 1700-1600 and 1560-1500 cm^{-1}), and NA: Nucleic acids (1250-1000 cm^{-1}). b) Approximation to the second derivative of the spectrum.

in absorbance/transmittance levels. Because saliva is made up of approximately 99% water [12], the amount of H-O-H bonds makes it difficult to appreciate the structure presented in Figure 1a., to solve this problem, it is necessary to submit the saliva sample to a drying process. Related bond mixing, the problem is that the more complex the sample composition is (proteins, organic molecules, and electrolytes for saliva [13]), the more complicated the spectrum becomes, making it difficult to associate a peak with a specific molecule. The above mentioned avoids the reliable identification of the molecule or molecules affected by a specific disease. Despite this, each component's number of bonds varies considerably depending on the macromolecular group to which they belong, which allows a specific region of the spectrum to be attributable reliably to a macromolecular group such as those indicated in Figure 1a. In studies such as those of H. Lin, the variability in absorbance/transmittance levels associated with age will have repercussions at the height of the spectrum (absorbance/trans-

mittance) [14], so a change in this factor is not necessarily an indicator of the disease. The differences in absorbances in spectra even of the same population, together with the overlap of the sample bonds, make it difficult to select a region with an exclusive pathology behavior.

In this sense, the machine learning area could present an interesting option to support preliminary clinical detection through FTIR spectrum. In works such as that of Alexandra S, *et al.* [15], it has provided an overview of the most promising techniques to be used, highlighting the use of artificial neural networks (ANN) compared to support vector machines (SVM) and techniques based on distances such as K-nearest neighbors, allowing to reach percentages of 100% in specificity for breast cancer detection, so it turns out to be the most promising technique. The main advantages of ANN and SVM are that they are non-linear techniques for the characterization of signals, while in ANN, non-linearity is achieved through the implementation of an activation function for its neurons, in SVM it is achieved through a transformation of the signal to a higher dimension using the technique called kernel trick. In a dimension equal to or greater than R3, the characterization of the signals using a hyperplane is less complex than in R2, allowing an accuracy of 100% in some cases, as presented by Alexandra S, *et al.*, [15].

REFERENCES

[1] Wang W, Xu Y, Gao R, Lu R, Han K, Wu G, Tan W. Detection of SARS-CoV-2 in Different Types of Clinical Specimens. JAMA [Internet]. 2020;323(18):1843-1844. Available from: https://dx.doi.org/10.1001%2Fjama.2020.3786

[2] World Health Organization. Health topics: Coronavirus. WHO [Internet]. 2020. Available from: *https://www.who.int/health-topics/coronavirus#tab=tab_1*

[3] Smith B. Fundamentals of Fourier Transform Infrared Spectroscopy. 2nd ed. Florida: Taylor and Francis Group; 2011. 1-17p.

[4] Beraki S, Aronsson F, Karlsson H, Ögren SO, Krostensson K. Influenza A virus infection causes alterations in expression of synaptic regulatory genes combined with changes in cognitive and emotional behaviors in mice. Molecular Psychiatry [Internet]. 2005;10:299-308. Available from: https://doi.org/10.1038/sj.mp.4001545

[5] Allison S, Carl G, Kavya R, Cargill KR, Cardnell RJ, et al. SARS-CoV-2 infection induces EMT-like molecular changes, including ZEB1-mediated repression of the viral receptor ACE2, in lung cancer models. bioRxiv [Preprint]. 2020;122291. Available from: https://doi.org/10.1101/2020.05.28.122291

[6] Expansión Política. Estos son los laboratorios validados para hacer pruebas de coronavirus. Expansión Política [Internet]. 2020; Available from: *https://politica.expansion.mx/mexico/2020/07/22/estos-son-los-laboratorios-validados-para-hacer-pruebas-de-coronavirus-covd-19*

[7] Paluszkiewicz C, Pięta E, Woźniak M, Piergies, N, et al. Saliva as a first-line diagnostic tool: A spectral challenge for identification of cancer biomarkers. Journal of Molecular Liquids [Internet]. 2020;307: 112961. Available from: https://doi.org/10.1016/j.molliq.2020.112961

[8] Wang X, Wu Q, Li C, Chou Y, Xu F, Zong L, Ge S. A study of Parkinson's disease patients' serum using FTIR spectroscopy. Infrared Physics & Technology [Internet]. 2020;106:103279. Available from: https://doi.org/10.1016/j.infrared.2020.103279

[9] Scott DA, Renaud DE, Krishnasamy S, Meriç P, Buduneli N, Çetinkalp Ş, Liu KZ. Diabetes-related molecular signatures in infraredspectra of human saliva. Diabetology & Metabolic Syndrome [Internet]. 2010;2: 2-9. Available from: https://doi.org/10.1186/1758-5996-2-48

[10] Roy S, Perez-Guaita D, Bowden S, Heraud P, Wood BR. Spectroscopy goes viral: Diagnosis of hepatitis B and C virus infection from human sera using ATR-FTIR spectroscopy. Clinical Spectroscopy [Internet]. 2019;1: 100001. Available from: https://doi.org/10.1016/j.clispe.2020.100001

[11] Arbely E, Khattari Z, Brotons G, Salditt T, Arkin IT. A Highly Unusual Palindromic Transmembrane Helical Hairpin Formed by SARS Coronavirus E Protein. Journal of Molecular Biology [Internet]. 2004;341(3): 769-779. Available from: https://doi.org/10.1016/j.jmb.2004.06.044

[12] Kaczor-Urbanowicz KE. Saliva Diagnostics. In Güvenç IA. Salivary Glands: New Approaches in Diagnostics and Treatment. London: InetchOpen; 2019 [Internet]. 51-52p. Available from: https://doi.org/10.5772/intechopen.68846

[13] Scully C, Posse JL, Diz Dios P. Saliva Protection and Transmissible Diseases. London: Academic Press; 2017. 1-2p.

[14] Lin H, Zhang Y, Wang Q, Li B, Huang P, Wang Z. Estimation of the age of human bloodstains under the simulated indoor and outdoor crime scene conditions by ATR-FTIR spectroscopy. Scientific Reports [Internet]. 2017;7:13254. Available from: https://doi.org/10.1038/s41598-017-13725-1

[15] Sala A, Anderson DJ, Brennan PM, Butler HJ, et al. Biofluid diagnostics by FTIR spectroscopy: A platform technology for cancer detection. Cancer Letters [Internet]. 2020;477(1): 122-130. Available from: https://doi.org/10.1016/j.canlet.2020.02.020

RESEARCH ARTICLE

Vol. 42 | No. 1 | **JANUARY - APRIL 2021** | pp 10-26

REVISTA MEXICANA DE Ingeniería Biomédica

dx.doi.org/10.17488/RMIB.42.1.2

E-LOCATION ID: 1051

The Impact of Staying at Home on Controlling the Spread of COVID -19: Strategy of Control

Zakary Omar, Bidah Sara, Rachik Mostafa

Laboratory of Analysis Modelling and Simulation, Department of Mathematics and Computer Science, Faculty of Sciences Ben M'Sik, Hassan II University of Casablanca

ABSTRACT

In this paper, we present a new mathematical model to describe the evolution of the COVID-19 in countries under the state of emergency. Where the COVID-19 pandemic is sweeping country after country. The Italian and Moroccan authorities have declared a state of emergency in response to the growing threat of this novel coronavirus (COVID-19) outbreak by March 09 and 20, respectively. In-state of emergency, citizens cannot go out to public spaces without special authorization from local authorities. But after all these efforts exerted by these authorities, the number of new cases of the COVID-19 continues to rise significantly, which confirms the lack of commitment of some citizens. First, we aim to investigate the cause of new infections despite all strategies of control followed in these countries including media reports, awareness, and treatment, self-distancing and quarantine, by estimating the number of these people who underestimate the lives and safety of citizens and put them at risk. To do this, we use real data of the COVID-19 in Italy and Morocco to estimate the parameters of the model, and then we predict the number of these populations. Second, we propose an optimal control strategy that could be the optimal and the efficient way for the Moroccan and Italian authorities and other countries to make the state of emergency more efficient and to control the spread of the COVID-19. The model is analyzed for both countries and then to compare the implications of the obtained results. Numerical examples are provided to illustrate the efficiency of the strategy of control that we propose and to show what would have been happened in Morocco and Italy if this strategy of control was applied early.

KEYWORDS: SARS-CoV-2; COVID-19; Mathematical model; Optimal control; Parameters estimation.

Corresponding author

TO: Zakary Omar

INSTITUTION: Hassan II University of Casablanca

ADDRESS: Av. Driss El Harti, Sidi Othmane, Faculty of Sciences Ben M'Sik, B. P. 7955, Casablanca, Morocco

E-MAIL: zakaryma@gmail.com

Received:

5 April 2020

Accepted:

25 June 2020

INTRODUCTION

Coronaviruses (CoV) are a large family of viruses that cause symptoms ranging from the common cold to more serious illnesses which mainly target the human respiratory system. Outbreaks of coronavirus (CoV), including severe acute respiratory syndrome (SARS) -CoV and the Middle East Respiratory Syndrome (MERS) -CoV, have been previously described as a major threat to public health [1].

Notwithstanding, COVID-19 is an infectious disease caused by a new coronavirus that has not been previously identified, called Severe Acute Respiratory Syndrome Coronavirus 2 (SARS-CoV-2), which was first called a new Coronavirus 2019 (2019-nCoV). The SARS-CoV-2 causes a flu-like respiratory illness such as coughing and fever and can even reach pneumonia [2]. This virus also demonstrated the ability to cause severe diseases among certain groups, including the elderly and individuals with health problems such as cardiovascular disease and diabetes [3].

COVID-19 spread from the city of Wuhan in December 2019 to other surrounding cities in China and then around the world. On March 11, 2020, the World Health Organization (WHO) declared the COVID-19 epidemic a pandemic, due to the steady increase in the number of confirmed cases worldwide, making the current coronavirus epidemic a global health threat.

By March 15, 2020, there had been more than 81,000 confirmed cases and more than 3,200 deaths in China due to the COVID-19 [2] [4]. As a result, international air traffic was reduced and the province of Hubei was closed around 3 weeks after the start of the COVID-19 epidemic.

Despite many countries have implemented flight restrictions to China, the daily reported cases increase significantly with and without a travel history to China. These developments lead to many concerns about potential unspecified and unreported international cases of COVID-19, which could lead to new local disease hotspots.

As of March 8, 2020, the total number of cases of COVID-19 had reached 80,859, including 3,100 deaths in China, the number of infections having rapidly increased after the massive growth of Hubei province, the epicenter of the disease [4]. Following the closure on February 15, 2020, the daily number of new cases reported in China began to decrease across the country, although Hubei Province reported 128 cases per day during the week of March 2-8 2020. As the epidemic continues to decrease in China, more than 700,000 cases of COVID-19 have been reported in more than 200 countries and territories outside of China, and hot spots of the disease have formed in the United States, Italy, Spain, Iran, Japan, Germany, France, and Morocco [4]. Given the continuing increase in confirmed cases of COVID-19 international, it is not clear how that further outbreaks of uncontrolled virus can be prevented.

In particular, Italy has become one of the countries most affected by COVID-19, as it has registered an increasing number of cases in recent days. Therefore, it is important to monitor the evolution of these epidemics and to assess the effects of various public health measures, including measures of quarantine and social distancing in real time. A potential scenario indicates that COVID-19 cases outside of China may spread and remain undetected for a period of time, delaying countermeasures in many countries. For example, in Italy, the first case of COVID-19 identified on January 31, 2020. After 20 days, the number of cases increased rapidly, resulting in 10,149 cases including 631 deaths on March 10, 2020. Some officials believe that the spread of the virus with the unreported or undetected cases is the cause of many confirmed cases, which means that at the time where the country realize the propagation of the COVID-19, there were many chains of transmission that are difficult to contain.

TABLE 1. Parameters description and values, initial data are corresponding to the 19 March 2020 for Morocco and January 31 for Italy [10].

Parameter	Description	Estimated values for Morocco	Estimated values for Italy
Γ_i	The recruitment rate	μN_i	μN_i
β	The infection rate	0.400000000163557	0.588699489613117
c	The reduced chances of a partially controlled individual to be infected	0.741241139596395	0.250892755438833
θ_1	The recruitment rate of susceptibles to the partially controlled class	0.0551738035422604	0.0200000000000233
θ_2	The recruitment rate of susceptibles to the totally controlled class	0.118144493564252	0.0300000000000233
μ	Natural death rate	0.00239997152652586	$1.94812917550124\times10^{-12}$
α	Death due to the infection	0.011000000000024	0.012174533433782
$\mathcal{T}$	Treatment rate	0.00201633557279791	0.00459260816896 83
γ	Recovery rate	0.0106341154978583	0.0114981237192988
ρ	Immunity loss rate	$2.43785373724565\times10^{-14}$	$1.98628130425312\times10^{-7}$
S_0	Initial susceptible population	34500000	60480000
P_0	Initial partially controlled population	0	0
C_0	Initial totally controlled population	0	0
I_0	Initial infected population	63	2
R_0	Initial recovered population	2	0
D_0	Initial dead population	2	0

On March 9, 2020, the government of Italy under Prime Minister Giuseppe Conte imposed a national quarantine, restricting population movement except for necessity, work and health conditions, in response to the growing epidemic of COVID-19 in the country. With additional lockdown restrictions mandated the temporary closure of non-essential shops and businesses. This measure is seen as a way to stop the spread of the virus that has hit Italy's aging population. Italy's Civil Protection Chief and Coronavirus Emergency Commissioner Angelo Borrelli said that 45% of those that have died were aged between 80 and 89, and 32% were in their seventies, 14% were over 90, 8% were in their sixties and 2% were aged between 50 to 59. Some bars and restaurants are still open, but they operate in limited hours without any commercial activities (except for supermarkets) that are scheduled to take place after 6 pm. Schools and universities are still closed; the national lockdown continues until April 3 [5].

The purpose of our study is to estimate those who do not respect the national closure and then endanger their lives and those of others, by creating arguments for not staying at home. Then we investigate the effect of this population on control measures against COVID-19, for example, awareness-raising programs, and treatment control even if there is no effective drug for COVID-19. To do this, first, we present a new mathematical model that describes the evolution of the COVID-19 in a population based on the classical SIRS model.

In this model we divide the population into six groups, Susceptible, Partially controlled, Totally controlled, Infected, Recovered, and Dead individuals. We incorporate in the model we propose the awareness programs and the treatment. In view of the fact that there is no effective vaccine for the COVID-19, the recovered people after a while become susceptible again.

Second, by using a nonlinear least-squares method, we estimate the model parameters by fitting the model to real data for both cases of Italy and Morocco to predict the situation in these countries by April 2020. Finally, we investigate several scenarios of optimal control strategies to discuss the best control that should have been followed to bring the situation under control in Italy and Morocco.

MATERIALS AND METHODS

Presentation of the model

Nowadays, diseases can move faster than ever because of the increasing movement of people between cities, regions, and countries. However, with digital technology, information can move faster, offering individuals and societies the opportunity to protect themselves before the disease itself occurs. Public awareness is important to manage the spread of infectious diseases. Individual measures, such as increasing attention to personal hygiene and avoiding crowds, can reduce the spread of the COVID-19.

Awareness programs also help to quickly identify and deal with new cases and facilitates group responses, such as school closings or public transit systems. Over the past two decades, with Internet availability and usage increased worldwide, people get information mainly through this novel alternative method [6].

Due to the lack of efficient treatment to the COVID-19, almost all authorities around the world adopt the national lockdown, social distancing, self-isolation, and national quarantine combined with great public awareness control strategies. In response to this pandemic, Chinese, Italian, Moroccan, and other governments have ordered a nationwide school closure as an emergency measure to prevent the spread of infection. The confinement of the population determines all hygiene and social dispersal procedures, known as "barriers," according to regulations related to maintaining one meter of distance between each other in public places, and bars and restaurants put tape on floors for their customers to follow, which has been defined at the national and local levels in response to the COVID-19 in Italy. In the hours following the nationwide lockdown announcement, supermarkets in Rome and Naples were hit by panic buying [7]. The Italian government was forced to reassure its citizens that the supermarkets would remain open and stored in the market around the clock [8].

Over the past two weeks, Italy has been divided between those who have been storing provisions, and one that has even ignored the basic rules, for example by organizing home parties in the affected areas.

The government hopes that the new measures will help curb these instincts [7]. Despite all of this, the number of confirmed COVID-19 cases still rising, this means that something is wrong. One possible reason is the lack of respect for the national quarantine and the underestimate of the contagiousness of the SARS-CoV-2.

During the first phase of the COVID19 epidemic, by improving the media reporting response rate to the severity of COVID-19 and by improving the response rate of public awareness of media reports, both can bring forward peak time and reduce peak size of infection significantly.

These results suggest that in addition to improving medical standards, media coverage can be seen as an effective means of mitigating the spread of the disease at the initial stage of an epidemic [9]. Therefore, we incorporate in our model the effects of media reporting and awareness programs to reduce the susceptible population.

All these efforts made by the authorities to aware people of the danger and rapid spread of this virus, motivated us to consider two new classes of people.

The first class is the aware individuals who know about the virus and the nationwide lockdown, called the Partially controlled individuals (P), because this population could not respect the national quarantine for one reason or another and could be considered as laws violator.

The second category is people who respect the national quarantine by staying at home from the start of the closure. This population is called a totally controlled population (C). Based on the classical compartmental models, we define the Susceptible (S), Infected (I), Recovered (R), and Dead (D) individuals and the rest of the classes studied here as follows:

- S: Susceptible people, people at risk or not yet infected and people who have not benefited from the awareness program.
- P: Partially controlled people, people who create arguments to leave their homes during the quarantine and can, therefore, be considered as people not respecting the quarantine.
- C: Totally controlled people, those who do not leave their home during quarantine and can, therefore, be considered as people respect the nationwide quarantine.
- I: Infected people, who are able to spread the COVID-19 to those in susceptible and partially controlled groups.
- R: Recovered people from the epidemic, but may return to the susceptible class due to the loss of individual immunity in the short term.
- D: The death toll from covid-19.

All these considerations lead to the following system of difference equations:

$$\begin{aligned} S_{i+1} &= S_i - \frac{\beta}{N_i} S_i I_i - \theta S_i + \Gamma_i - \mu S_i + \rho R_i \\ P_{i+1} &= P_i - \frac{c\beta}{N_i} P_i I_i + \theta_1 S_i - \mu P_i \\ C_{i+1} &= C_i + \theta_2 S_i - \mu C_i \\ I_{i+1} &= I_i + \frac{\beta}{N_i}(S_i + cP_i) I_i - \gamma I_i - \mu I_i - \alpha I_i - \mathcal{T} I_i \\ R_{i+1} &= R_i + \mathcal{T} I_i + \gamma I_i - \mu R_i - \rho R_i \\ D_{i+1} &= D_i + \alpha I_i \end{aligned} \tag{1}$$

With initial conditions $S_0 \geq 0$, $P_0 \geq 0$, $C_0 \geq 0$, $I_0 \geq 0$, $R_0 \geq 0$ and $D_0 \geq 0$ and where $N_i = S_i + P_i + C_i + I_i + R_i$ is the total size of the population at the instant i. Without loss of generality, we consider the recruitment rate equal to the natural death rate due to the restricted time window of the epidemic, that is $\Gamma_i = \mu N_i$, is the newborn people which considered susceptible individuals, μ is the natural death rate.

After one unit of time, susceptible individuals may remain in the susceptible compartment, or become infected with a contact with infectious individuals ($\frac{\beta}{N_i} S_i I_i$) and move to the infectious compartment or benefit from awareness (θS_i) and move to the partially ($\theta_1 S_i$) or totally controlled ($\theta_2 S_i$) compartment, or die at a per capita μS_i. Where β is the infection transmission rate, and $\theta = \theta_1 + \theta_2$ defining the control of media report and awareness programs, where θ_1 is the recruitment rate of susceptibles to the partially controlled class, and θ_2 is the recruitment rate of susceptibles to the totally controlled class.

Partially controlled individuals may stay in P compartment or get infected with a reduced probability with a contact with infectious people ($\frac{c\beta}{N_i} P_i I_i$) and move to the infected compartment, or die.

Where "c" modeling the reduced chances of a partially controlled individual to be infected where $0 \leq c \leq 1$.

The totally controlled individuals never leave their compartment until they die.

The infected individuals may stay in the infected compartment or get recovered at per capita γI_i or treated at per capita TI_i and move to the recovered compartment, or die due to the infection at a per capita αI_i and move to the dead compartment, or die naturally.

The recovered individuals may remain in its compartment or lose the immunity and move to the susceptible compartment at a per capita ρR_i, or die. Where T is the treatment rate, α is the infection death rate, γ is the recovery rate and ρ is the losing removal individuals' immunity rate.

We note that the population size N_i is not constant in time i, in fact

$$\begin{aligned} N_{i+1} &= S_{i+1} + P_{i+1} + C_{i+1} + I_{i+1} + R_{i+1} \\ N_{i+1} &= N_i + \Gamma_i - \mu N_i - \alpha I_i \\ N_{i+1} &= N_i - \alpha I_i \end{aligned} \tag{2}$$

Hence the population decreases until the end of the epidemic. A summary of the description and values of the parameters is given in Table 1.

Estimation of the parameters

In response to the current public health emergency, the CSSE Center for Systems Science and Engineering at Johns Hopkins University has developed and hosted an interactive web dashboard to view and follow up on reported cases in real-time [11].

The dashboard was first released on January 22 and shows the location and number of confirmed COVID-19 cases, deaths, and recoveries for all affected countries. It was developed to provide researchers, public health authorities and the general public with an easy-to-use tool for tracking disease outbreaks when they occur. Besides, all the data collected and displayed is provided free of charge in the GitHub repository [10].

Every 15 minutes, the cumulative number of DXY (An online platform run by members of the Chinese medical community, [12]) cases is updated for all provinces in China and the affected countries and regions. Case numbers are updated manually throughout the day for countries and regions outside of China (including Hong Kong, Macao, and Taiwan) and when new cases are identified. Before manually updating the dashboard, case numbers are confirmed using regional and local health services, the China Disease Control Center (CCDC) [13], Hong Kong Department of Health [14], Macau Government [15], Taiwan CDC [16], European CDC (ECDC) [17], the World Health Organization (WHO) [4], as well as city and state-level health authorities.

Our study focuses on the February and March period concerning the real data for Italy, and on the March period concerning the Moroccan data. This is due to the rapid response of the Moroccan government by applying the nationwide quarantine after only 63 cases and 2 deaths on March 20 compared to Italy, which announced the closure of the country after 6,387 cases and 366 deaths on March 9.

To verify the reality of that model, we use nonlinear least-squares regression to fit the model to actual observations. Therefore, the following process has been followed for parameters estimation:

With MATLAB, the system of difference equations is solved numerically, the initial values being chosen for the parameters and the case variables of table 1. The results of the model are compared with field data and the Levenberg-Marquardt optimization algorithm defines a new set of parameter values with the results of the model better suited to field data.

After determining the values of the new parameters with this optimizer, the system of difference equations is solved numerically using the value of these new parameters and the results of the model are again

compared with field data. This iteration process continues between the updating of the parameters and the numerical solutions of a system of difference equations using iterative diagrams until the criteria for convergence of the parameters are fulfilled. In this process of estimating the parameters, around one thousand values, are chosen using a random process for each of the parameters to be estimated.

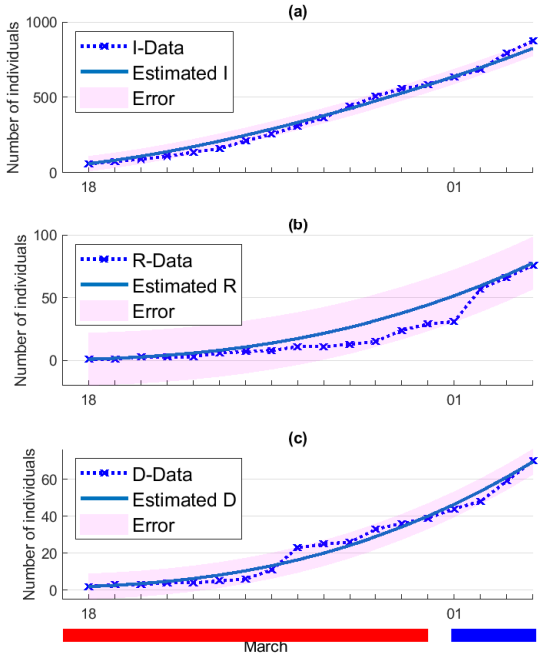

FIGURE 1. Data fitting for the data from March 18 to April 04, 2020 of Morocco. The markers represent (a) the active number of confirmed cases, (b) the number of recovereds, (c) the number of deaths. The solid curves are the best fitting curves of model (1) to these data.

In Figure 1 we can see that our model fits correctly the real data of Morocco, especially the data of infected cases, see the sub-figure (a). In (b), we can see the estimation of the R function where it can be seen that there are some errors plotted with the filled area, while in (c) we can see the estimation of the D function with some errors between a range plotted with the filled area. To provide a prediction based on the estimated parameters given in Table 1 we simulate our model from the beginning of the quarantine on 19 March to 07 May, see Figure 2. This figure depicts the continuous increase of the three functions I, R and D, albeit at a weak form they wouldn't stop.

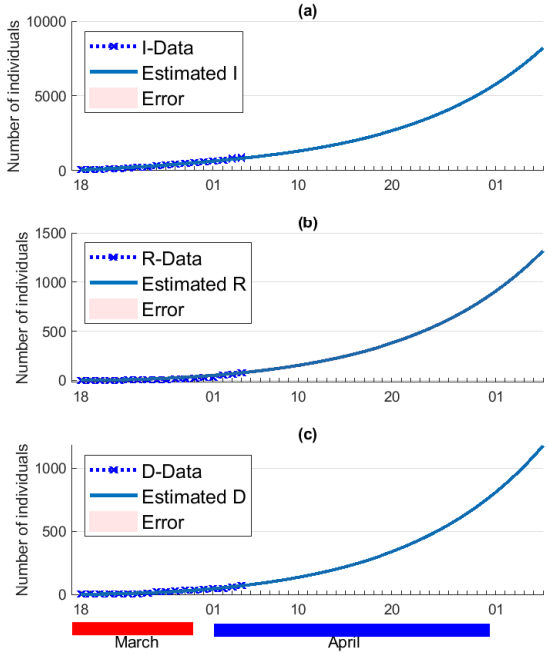

FIGURE 2. Estimating the situation of COVID-19 in Morocco by April and the first week of May 2020. The markers represent (a) the active number of confirmed cases, (b) the number of recovereds, (c) the number of deaths. The solid curves are the best fitting curves of model (1) to these data.

Figure 3 depicts the estimation of the controlled population, where it can be seen that after about 10 days all the population is considered controlled where the susceptible population takes about zero values at the end of April, and the partially controlled and the totally controlled population rise towards about 15 million and 20 million respectively. That figure shows the efficiency of the awareness control in reaching all the population, but it can be seen that this control is not sufficient to bring the situation under control. The Moroccan authorities must apply more serious movements restriction to reduce the number of partially controlled population which represents the high-risk population.

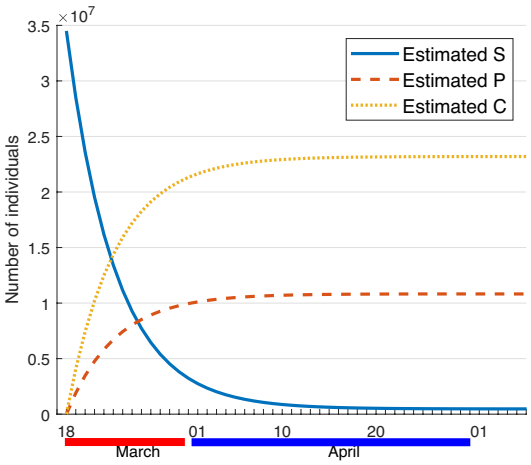

FIGURE 3. Estimating the high-risk population in Morocco by April and the first week of May 2020.

To show the impact of this population on the control of the COVID-19 in Morocco, we consider a scenario when all the population respects the quarantine which means that there is no partially controlled population, that is $\theta_1 = 0$. We can see from Figure 4 that from the beginning of the quarantine, the number of infected cases starts to decrease continuously, while the number of dead people would not exceed 40 individuals. But this scenario is more theoretical than real, since the total lockdown is more costly and can lead to serious economical damages.

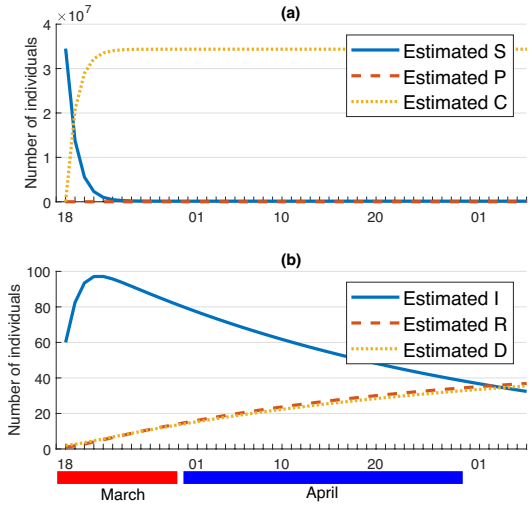

FIGURE 4. Simulation of the model (1) with $\theta_1 = 0$ and $\theta_1 = 0.6$.

This simulation shows that it is necessary to think about controlling this population to achieve more satisfactory results. To investigate a more realistic scenario we consider in the following section an optimal control approach that aims to stop the infection process with an optimal cost.

In Figure 5 we can see that our model also fits correctly the real data of Italy from January 31 to March 30, especially the data of infected cases, see the sub-figure (a). In (b), we can see the estimation of the R function where it can be seen that there are some errors between a range of ±875 individuals, while in (c) we can see the estimation of the D function with some errors between a range of ±725.

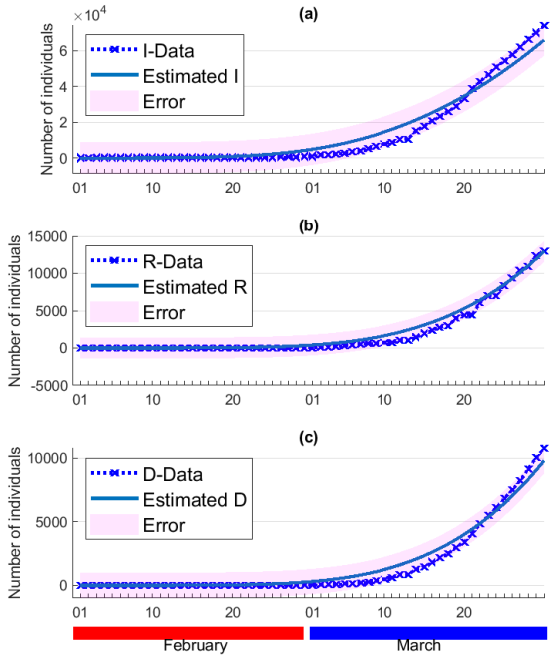

FIGURE 5. Data fitting for the data from February first to March 31, 2020 of Italy. The markers represent (a) the active number of confirmed cases, (b) the number of recovereds, (c) the number of deaths. The solid curves are the best fitting curves of model (1) to these data.

To provide a prediction based on the estimated parameters given in Table 1 we simulate our model from January 31 to May 07, see Figure 6.

This figure depicts the continuous increase of the three functions I, R and D, which would reach huge numbers by the end of April.

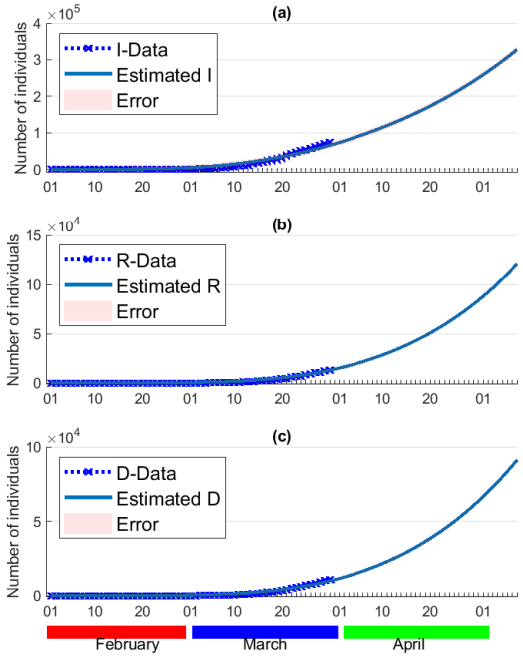

FIGURE 6. Estimating the situation of COVID-19 in Italy from February to the first week of May 2020. The markers represent (a) the active number of confirmed cases, (b) the number of recovereds, (c) the number of deaths. The solid curves are the best fitting curves of model (1) to these data.

Figure 7 depicts the estimation of the controlled populations, where it can be seen that the susceptible population decreases which show the effect of the awareness programs on increasing the number of controlled individuals. While the number of partially and totally controlled individuals increases slightly, which can be interpreted by the non-serious behavior of people regarding the spread of this pandemic.

This explains the high number of infections in Italy and the insufficiency of the control strategy pursued by the Italian authorities so far. In the following section, we will discuss the strategy of control that should have been applied in Italy to avoid this huge number of deaths and infections.

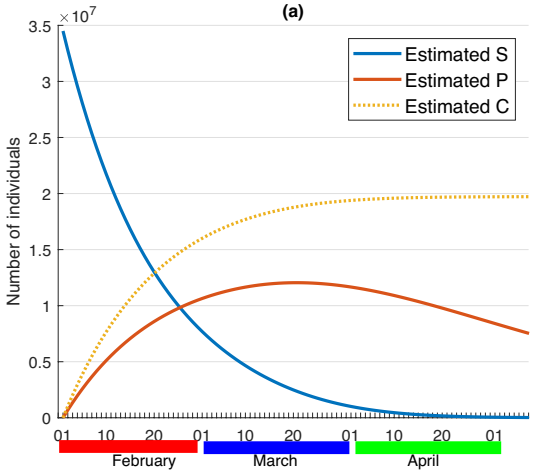

FIGURE 7. Estimating the high-risk population in Italy from February to the first week of May 2020.

Because the residuals need to be determined numerically, we examine the accuracy of the normality of the estimation of the parameters. In order to carry out this examination, we generate the residuals of the infected, removed and dead populations for Morocco and Italy.

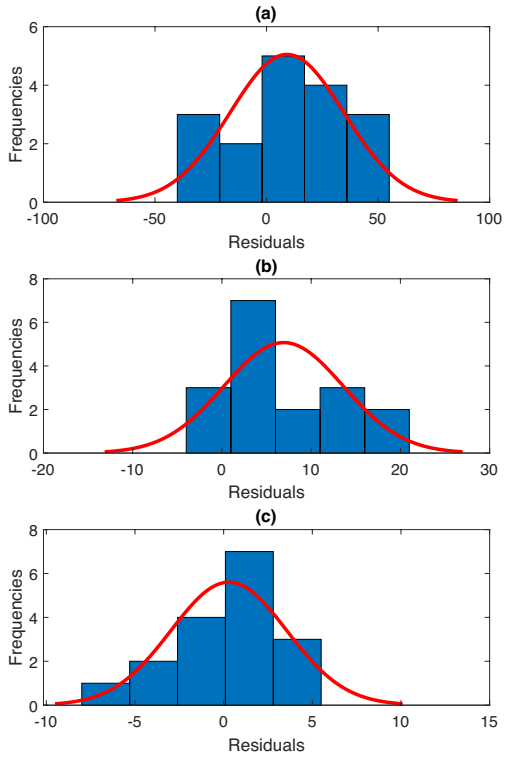

FIGURE 8. Residuals of the parameters estimation for Morocco.

Figure 8 displays the corresponding histograms of I_k - I_k^{data} in (a) and R_k - R_k^{data} in (b) and D_k - D_k^{data} in (c) for the estimation of the parameters for Morocco with their corresponding normal distributions. While Figure 9 depicts the corresponding histograms of I_k - I_k^{data} in (a) and R_k - R_k^{data} in (b) and D_k - D_k^{data} in (c) for the estimation of the parameters for Italy with their corresponding normal distributions. These figures show that the estimated parameters are reliable and predict correctly the observed data, especially the number of infections.

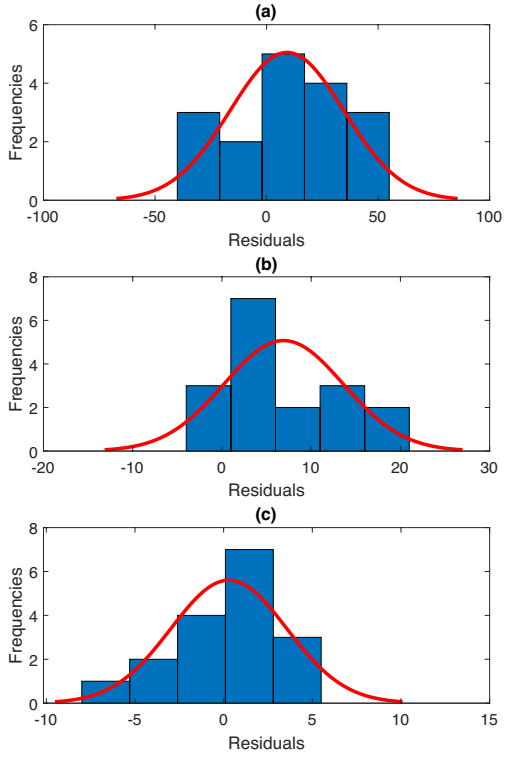

FIGURE 8. Residuals of the parameters estimation for Italy.

The objective of this part of the article is not to predict what will happen in the coming months but to validate the proposed model by fitting the model's outputs to real data, then to estimate the high-risk population in these countries during the period used to estimate the parameters. Therefore, contribute to the control of this pandemic by suggesting an optimal control strategy to make the national closure more effective in reducing new infections and saving more lives. Knowing that these countries could use additional controls such as new treatment, massive tests, the obligation of masks, or more restrictions of movement, after the period of estimation of the parameters, which would make the predictions of our model exaggerated.

An optimal control approach

Authorities provide all necessary assistance to residents to stay at home during the quarantine period. By spending financial values on poor families and by dispensing certain useless occupations in the course of this period. Consequently, people who break quarantine can be considered as violating the laws, as they will take the maximum penalties, which reach the prison.

In this section, we introduce in the model a control variable that represents the previous severe reactions of the authorities against people who do not respect the national quarantine, denoted by u_i. Thus, the controlled model is given by

$$\begin{aligned}
S_{i+1} &= S_i - \frac{\beta}{N_i} S_i I_i - \theta S_i + \Gamma_i - \mu S_i + \rho R_i \\
P_{i+1} &= P_i - \frac{c\beta}{N_i} P_i I_i + \theta_1 S_i - \mu P_i - u_i P_i \\
C_{i+1} &= C_i + \theta_2 S_i - \mu C_i + u_i P_i \\
I_{i+1} &= I_i + \frac{\beta}{N_i}(S_i + cP_i) I_i - \gamma I_i - \mu I_i - \alpha I_i - \mathcal{T} I_i \\
R_{i+1} &= R_i + \mathcal{T} I_i + \gamma I_i - \mu R_i - \rho R_i \\
D_{i+1} &= D_i + \alpha I_i
\end{aligned} \tag{3}$$

With initial conditions $S_0 \geq 0$, $P_0 \geq 0$, $C_0 \geq 0$, $I_0 \geq 0$, $R_0 \geq 0$ and $D_0 \geq 0$. The main objective of all the countries affected by COVID-19 is to reduce as much as possible the infected and partially controlled people while reducing the costs of control u, which can be translated mathematically to the seek of an optimal control u^* such that:

$$\mathcal{J}(u^*) = \min_{u \in \mathcal{U}} \mathcal{J}(u) \tag{4}$$

where $\mathcal{J}$ is the functional defined by:

$$\mathcal{J}(u) = K_1 I_T + K_2 P_T + \sum_{i=0}^{T-1} K_1 I_i + K_2 P_i + \frac{K_3}{2} u_i^2 \tag{5}$$

and where the admissible control set $\mathcal{U}$ is defined by:

$$\begin{aligned}\{u \in \mathbb{R}^T / u_{min} \leq u_i \leq u_{max}, \forall i = 0, \ldots, T, \ 0 \\ \leq u_{min} \leq u_{max} \leq 1\}\end{aligned} \tag{6}$$

K_1, K_2 and K_3 represent constant severity weights associated with functions I, P, and u, respectively.

Existence of the optimal control

Theorem. There exists an optimal control $u^* \in \mathcal{U}$ such that

$$\mathcal{J}(u^*) = min\{\mathcal{J}(u)/u \in \mathcal{U}\}$$

subject to the control system (3) and initial conditions.

Proof. Since the parameters of the system are bounded and there are a finite number of time steps, that is S, P, C, I, R and D are uniformly bounded for all uin the control set $\mathcal{U}$, thus $\mathcal{J}(u)$is also bounded for all $u \in \mathcal{U}$. Which implies that $inf_{u\in\mathcal{U}}\ \mathcal{J}(u)$ is finite, and there exists a sequence $u^n \in \mathcal{U}$ such that

$$\lim_{n\to+\infty} \mathcal{J}(u^n) = \inf_{u\in\mathcal{U}} \mathcal{J}(u)$$

and corresponding sequences of states, S^n, P^n, C^n, I^n, R^n and D^n.

Since there is a finite number of uniformly bounded sequences, there exists $u^* \in \mathcal{U}$ and S^*, P^*, C^*, I^*, R^* and D^* such that, on a sequence,

$$\begin{aligned} u^n &\to u^* \\ I^n &\to I^* \\ S^n &\to S^* \\ R^n &\to R^* \\ F^n &\to F^* \end{aligned}$$

Finally, due to the finite dimensional structure of the system (2) and the objective function $\mathcal{J}(u)$, u^* is an optimal control with corresponding states S^*, P^*, C^*, I^*, R^* and D^*. Which complete the proof.

Characterization of the optimal control

By using a discrete version of the Pontryagin's maximum principle [18] [19] [20] [21] [22], we derive necessary conditions for our optimal control problem. For this purpose, we define the Hamiltonian as:

$$\begin{aligned}\mathcal{H}(i) &= K_1 I_i + K_2 P_i + \frac{K_3}{2} u_i^2 \\ &+ \zeta_{1,i+1}\left[S_i - \frac{\beta}{N_i} S_i I_i - \theta S_i + \Gamma_i - \mu S_i + \rho R_i\right] \\ &+ \zeta_{2,i+1}\left[P_i - \frac{c\beta}{N_i} P_i I_i + \theta_1 S_i - \mu P_i - u_i P_i\right] \\ &+ \zeta_{3,i+1}[C_i + \theta_2 S_i - \mu C_i + u_i P_i] \\ &+ \zeta_{4,i+1}\left[I_i + \frac{\beta}{N_i}(S_i + cP_i) I_i - \gamma I_i - \mu I_i - \alpha I_i - \mathcal{T} I_i\right] \\ &+ \zeta_{5,i+1}[R_i + \mathcal{T} I_i + \gamma I_i - \mu R_i - \rho R_i] \\ &+ \zeta_{6,i+1}[D_i + \alpha I_i]\end{aligned} \tag{7}$$

Theorem. Given an optimal control u^* and solutions S^*, P^*, C^*, I^*, R^* and D^*, there exists $\zeta_{k,i}$, $i = 0 \ldots T - 1$, k = 1,2,...,6, the adjoint variables satisfying the following equations:

$$\begin{aligned}\Delta\zeta_{1,i} &= \zeta_{4,i+1}\left(\frac{\beta I_i S_i}{N_i^2} - \frac{\beta I_i}{N_i} + \frac{c\beta I_i P_i}{N_i^2}\right) - \zeta_{3,i+1}\theta_2 \\ &+ \zeta_{1,i+1}\left(\theta_1 + \theta_2 + \frac{\beta I_i}{N_i} - \frac{\beta I_i S_i}{N_i^2} - 1\right) \\ &- \zeta_{2,i+1}\left(\theta_1 + \frac{c\beta I_i P_i}{N_i^2}\right) \\ \Delta\zeta_{2,i} &= \zeta_{2,i+1}\left(\mu + u_i + \frac{c\beta I_i}{N_i} - \frac{c\beta I_i P_i}{N_i^2} - 1\right) - K_2 \\ &+ \zeta_{4,i+1}\left(\frac{\beta I_i S_i}{N_i^2} - \frac{c\beta I_i}{N_i} + \frac{c\beta I_i P_i}{N_i^2}\right) - \zeta_{3,i+1} u_i \\ &- \zeta_{1,i+1}\left(\mu + \frac{I_i S_i \beta}{N_i^2}\right) \\ \Delta\zeta_{3,i} &= \zeta_{3,i+1}(\mu - 1) + \zeta_{4,i+1}\left(\frac{c\beta I_i S_i}{N_i^2} + \frac{c\beta I_i P_i}{N_i^2}\right) \\ &- \zeta_{1,i+1}\left(\mu + \frac{I_i S_i \beta}{N_i^2}\right) - \frac{c\beta I_i P_i \zeta_{2,i+1}}{N_i^2}\end{aligned} \tag{8}$$

$$
\begin{aligned}
\Delta\zeta_{4,i} &= \zeta_{1,i+1}\left(\frac{S_i\beta}{N_i}-\frac{I_iS_i\beta}{N_i^{\,2}}-\mu\right)-K_1-\alpha\zeta_{6,i+1}\\
&\quad+\zeta_{2,i+1}\left(\frac{P_i\beta c}{N_i}-\frac{I_iP_i\beta c}{N_i^{\,2}}\right)\\
&\quad+\zeta_{4,i+1}(\mathcal{T}+\alpha+\gamma+\mu-\frac{S_i\beta}{N_i}+\\
&\quad\frac{I_iS_i\beta}{N_i^{\,2}}-\frac{P_i\beta c}{N_i}+\frac{I_iP_i\beta c}{N_i^{\,2}}-1)\\
&\quad-\zeta_{5,i+1}(\mathcal{T}+\gamma)\\
\Delta\zeta_{5,i} &= \zeta_{5,i+1}(\mu+\rho-1)-\zeta_{1,i+1}\left(\mu+\rho+\frac{I_iS_i\beta}{N_i^{\,2}}\right)\\
&\quad+\zeta_{4,i+1}\left(\frac{I_iS_i\beta}{N_i^{\,2}}+\frac{I_iP_i\beta c}{N_i^{\,2}}\right)-\frac{I_iP_i\beta c\zeta_{2,i+1}}{N_i^{\,2}}\\
\Delta\zeta_{6,i} &= -\zeta_{6,i+1}
\end{aligned}
\tag{8}
$$

where $\zeta_{1,T}=\zeta_{3,T}=\zeta_{5,T}=\zeta_{6,T}=0$, $\zeta_{2,T}=K_2$, $\zeta_{4,T}=K_1$ are the transversality conditions. In addition

$$
\begin{aligned}
u_i^* &= min\{max\{u_{min},\frac{P_i(\zeta_{2,i+1}-\zeta_{3,i+1})}{K_3}\},u_{max}\}\\
&\quad,i=0,\dots,T-1
\end{aligned}
\tag{9}
$$

Proof. Using the discrete version of the Pontryagin's maximum principle [18] [19], we obtain the following adjoint equations:

$$
\begin{aligned}
\Delta\zeta_{1,i} &= -\frac{\partial\mathcal{H}}{\partial S_i}\\
&= \zeta_{4,i+1}(\frac{\beta I_iS_i}{N_i^{\,2}}-\frac{\beta I_i}{N_i}+\frac{c\beta I_iP_i}{N_i^{\,2}})-\zeta_{3,i+1}\theta_2\\
&\quad+\zeta_{1,i+1}(\theta_1+\theta_2+\frac{\beta I_i}{N_i}-\frac{\beta I_iS_i}{N_i^{\,2}}-1)\\
&\quad-\zeta_{2,i+1}(\theta_1+\frac{c\beta I_iP_i}{N_i^{\,2}})\\
\Delta\zeta_{2,i} &= -\frac{\partial\mathcal{H}}{\partial P_i}\\
&= \zeta_{2,i+1}(\mu+u_i+\frac{c\beta I_i}{N_i}-\frac{c\beta I_iP_i}{N_i^{\,2}}-1)-K_2\\
&\quad+\zeta_{4,i+1}(\frac{\beta I_iS_i}{N_i^{\,2}}-\frac{c\beta I_i}{N_i}+\frac{c\beta I_iP_i}{N_i^{\,2}})-\zeta_{3,i+1}u_i\\
&\quad-\zeta_{1,i+1}(\mu+\frac{I_iS_i\beta}{N_i^{\,2}})\\
\Delta\zeta_{3,i} &= -\frac{\partial\mathcal{H}}{\partial C_i}\\
&= \zeta_{3,i+1}(\mu-1)+\zeta_{4,i+1}(\frac{c\beta I_iS_i}{N_i^{\,2}}+\frac{c\beta I_iP_i}{N_i^{\,2}})\\
&\quad-\zeta_{1,i+1}(\mu+\frac{I_iS_i\beta}{N_i^{\,2}})-\frac{c\beta I_iP_i\zeta_{2,i+1}}{N_i^{\,2}}\\
\Delta\zeta_{4,i} &= -\frac{\partial\mathcal{H}}{\partial I_i}\\
&= \zeta_{1,i+1}(\frac{S_i\beta}{N_i}-\frac{I_iS_i\beta}{N_i^{\,2}}-\mu)-K_1-\alpha\zeta_{6,i+1}\\
&\quad+\zeta_{2,i+1}(\frac{P_i\beta c}{N_i}-\frac{I_iP_i\beta c}{N_i^{\,2}})\\
&\quad+\zeta_{4,i+1}(\mathcal{T}+\alpha+\gamma+\mu-\frac{S_i\beta}{N_i}+\\
&\quad\frac{I_iS_i\beta}{N_i^{\,2}}-\frac{P_i\beta c}{N_i}+\frac{I_iP_i\beta c}{N_i^{\,2}}-1)\\
&\quad-\zeta_{5,i+1}(\mathcal{T}+\gamma)\\
\Delta\zeta_{5,i} &= -\frac{\partial\mathcal{H}}{\partial R_i}\\
&= \zeta_{5,i+1}(\mu+\rho-1)-\zeta_{1,i+1}(\mu+\rho+\frac{I_iS_i\beta}{N_i^{\,2}})\\
&\quad+\zeta_{4,i+1}(\frac{I_iS_i\beta}{N_i^{\,2}}+\frac{I_iP_i\beta c}{N_i^{\,2}})-\frac{I_iP_i\beta c\zeta_{2,i+1}}{N_i^{\,2}}\\
\Delta\zeta_{6,i} &= -\frac{\partial\mathcal{H}}{\partial D_i}= -\zeta_{6,i+1}
\end{aligned}
$$

With $\zeta_{1,T}=\zeta_{3,T}=\zeta_{5,T}=\zeta_{6,T}=0$, $\zeta_{2,T}=K_2$,$\zeta_{4,T}=K_1$.

To obtain the optimality conditions we take the variation with respect to controls (u_i and v_i) and set it equal to zero

$$\frac{\partial\mathcal{H}}{\partial u_i}=P_i\zeta_{2,i+1}-P_i\zeta_{3,i+1}-K_3u_i=0$$

Then we obtain the optimal control

$$u_i=\frac{P_i(\zeta_{2,i+1}-\zeta_{3,i+1})}{K_3}$$

By the bounds in $\mathcal{U}$ of the control in the definitions (6), it is easy to obtain u_I^*in the following form

$$
\begin{aligned}
u_i^* &= min\{max\{u_{min},\frac{P_i(\zeta_{2,i+1}-\zeta_{3,i+1})}{K_3}\},u_{max}\}\\
&\quad,i=0,\dots,T-1
\end{aligned}
$$

RESULTS AND DISCUSSION

Numerical simulation

Here, we provide the numerical simulations related to the optimization problem mentioned above. We write the code in MATLAB™ and simulate our results using different data from Table 1. The optimality systems are solved based on an iterative discrete method which converges after an appropriate test similar to that for FBSM. The state system is resolved with the initial assumption forward in time, then the adjoint system is solved backward in time due to the transversality conditions. Next, we update the optimal control values using the state and co-state values obtained in the previous steps. Finally, we implement the previous steps until the tolerance standard is reached.

To demonstrate the efficiency of the optimal strategy of control that we propose, and to give a comparison with the case when there is no optimal control, we choose to simulate the controlled model in the months of February, March, and April in the case of Italy, and in the months of March and April in the case of Morocco.

Our model correctly corresponds to the Italian data (see Figure 5) and predicts that the number of COVID-19 cases will continue to increase if the Italian authorities do not take other measures such as the appearance of a new treatment, see Figure 6. While in Figure 10 we can see that the number of infections reaches the peak by about 9000 infected individuals on April first, and then starts to decrease. And the number of deaths does not exceed 6000 (see the sub-figure (b)) by the end of April. By following these strategies of control, the partially controlled population remains almost null, see the sub-figure (a), which gives the healthcare authorities the necessary time to save more lives. From the sub-figure (c) we can see that by May first, there is no more need for this control, where the function u takes null values since that time.

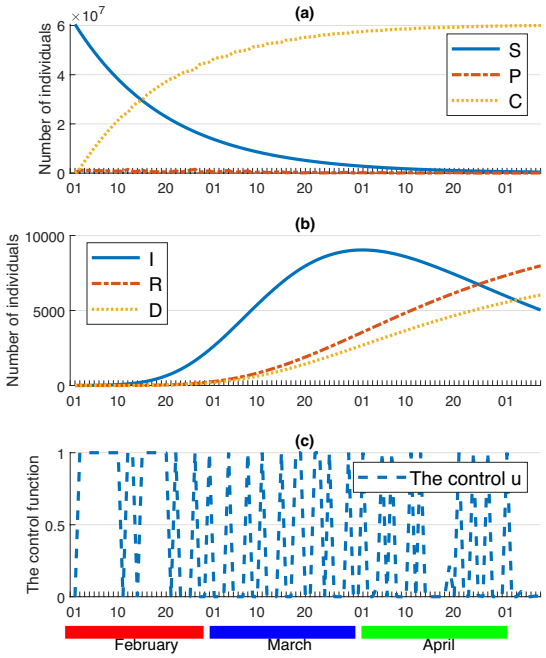

FIGURE 10. The controlled model (2) simulated with the parameters of Italy. (a) The three functions of susceptible *S*, partially controlled *P*, and totally controlled *C* population. (b) The three functions of infected *I*, recovered *R*, and dead *D* population. (c) The control function.

Figure 11 depicts the efficiency of the control u in reducing the number of partially controlled individuals, and increasing the number of totally controlled people (a) in Morocco, and then reducing the number of new cases of infection, and the number of deaths (b), which would not exceed 150 by 07 of May, while this number exceeds 1000 dead individuals at the beginning of May, in the case when there is no control u, see (c) of Figure 2. While it can be seen, from the sub-figure (c) of Figure 11, that the control function u takes discrete values separated by null values, while we can see that this control is needed until the end of this simulation. To achieve this satisfactory results, the control starts from the beginning of the closure to inverse the direction of the course of events, while the number of the partially controlled people rise to about 11 million individuals and stabilize there until the end of April, when the control u is not applied yet, see

Figure 3. But, when the optimal control u is applied, the number of the partially controlled people starts decreasing towards zero to take almost null values by about April first, see (a) of the Figure 11.

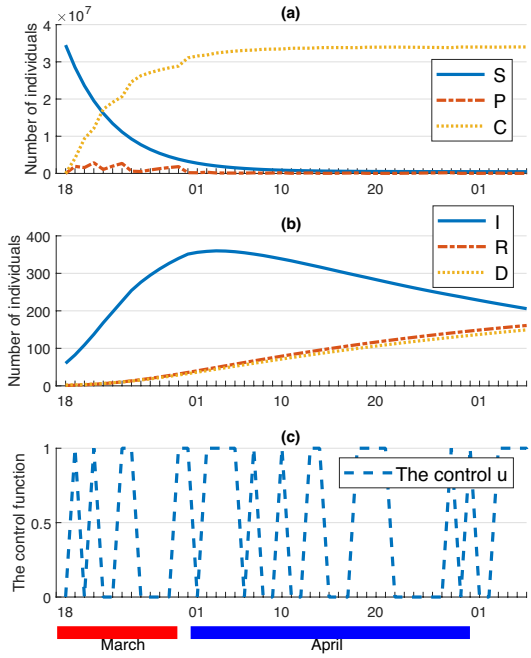

FIGURE 11. The controlled model (2) simulated with the parameters of Morocco. (a) The three functions of susceptible *S*, partially controlled *P*, and totally controlled *C* population. (b) The three functions of infected *I*, recovered *R*, and dead *D* population. (c) The control function.

Discussion

In recent work, Zhou et al. in [9] studied the effects of media reports on mitigating the spread of COVID-19 in the early stage of an outbreak, where the authors discussed a mathematical model that provided a detailed scheme in the early stage of the COVID-19 outbreak, and included the ODE model. Their findings indicate that, in addition to improving medical standards, media coverage can be considered an effective way to mitigate the spread of the disease in the first stage of the epidemic. Based on this fact, we incorporate in our model the effect of media reporting and the awareness programs to reduce the number of susceptible population (the parameter $\theta = \theta_1+\theta_2$), but our principal aim is to estimate the high-risk population in countries under quarantine (lockdown) not in the early phase of the propagation of the pandemic compared to the model proposed in [9], and then to contribute in the control of this disease.

Other work presented in [23] assesses different scenarios, based on an estimate of the number of identified and unidentified cases, and studies the effectiveness of different policy responses to contain the epidemic in Iran. The authors have shown that in many cases the number of unidentified cases, including asymptomatic individuals, can be much higher than the reported numbers, and the control strategy they suggest is to combine effective social spacing to extensive testing, even for those without symptoms and isolate active cases. This control strategy can work in Italy; however, it is not applicable in developing countries like Morocco due to the limited medical protection equipment, fragile health resources and infrastructures which do not allow a number of enough daily tests. Whereas, in our control strategy, we suggest only optimal self-isolation to make the state of emergency more efficient and this shows satisfactory results in Italy and Morocco regardless of medical resources.

Tian et al. in [24], adopted the interrupted time series method and developed the SEI / QR model for analyzing data from Anhui in China, which is divided into three phases. During the first phase, general awareness of the severity of the disease was low and infections might be treated like the common cold. In the second phase, the public began to realize the severity of the epidemic after the closure of Wuhan and the closure in other cities in Hubei soon after. In the third stage, central quarantine management measures were adopted for close communication in Anhui and resulted in a decrease in the possibilities of communication between residents. The authors concluded that the closure of Wuhan and the timely central quaran-

tine procedures in Anhui had significantly reduced the speed of transmission of COVID-19. This work focuses on the different stages of the detection of epidemics in China, but the virus and the disease of SARS-CoV-2 (COVID-19) were identified before the declaration of the first cases in Italy and Morocco, which makes the analysis of [24] not applicable in these countries.

All the above-mentioned models are continuous, but the model we propose here is in discrete-time. One of the reasons for the rise of discrete time models is that these models have advantages for describing infectious diseases, since epidemic data are generally collected in separate time units, which would make them easier to use and ease with which data can be compared to simulated results.

To avoid what are the things going to in other countries, the optimal and efficient way to bring the situation under control is the optimal control strategy we propose here. It can be seen that in this strategy of control, there is no need for more medical care or medical equipment. The Moroccan authorities need to use restraining measures, stipulated in the decree by law, to deter violators, who underestimate the lives and safety of citizens, and put them at risk.

The absence of anti-COVID-19 treatment and an effective vaccine against COVID-19, and limited medical resources are all factors that make it more difficult to stem the transmission of this pandemic. Therefore, it is necessary to consider other means of interventions. Travel restrictions have been implemented in most countries of the world, effectively reducing the movement of millions, quarantine, and health emergencies require people to stay indoors during the COVID-19 outbreak to reduce contact with others, which already contributes to the prevention and control of the disease, with all these strategies of control, the new infection cases still recorded in Italy and Morocco which give us the opportunity to contribute in the containment of this dangerous pandemic by proposing the optimal strategy of control that appears to be more efficient by bringing forward the peak and reducing the size of the infection peak in both countries under investigation.

Many countries have taken advantage of the experience of China and Italy in fighting this pandemic. This saved him time to try to contain the severe spread of the COVID-19 infection. And learned them that this spare time must be used efficiently and effectively. Morocco is one of these countries, where the emergency home education plan was meticulously implemented [25]. Schools and teachers make tremendous efforts at all levels to create and deliver online courses via TV and Internet broadcasts in record time. The new virtual semester has just begun across the country, and various online courses are offered in a good manner [26]. These measures help alleviate the concerns of many parents about the educational attainment of their children by ensuring that school learning is not greatly interrupted and then help people to stay at home. Financial aid for poor families and for hanging crafts. Imposing early quarantine. Some posts went so far as to say that Morocco preferred its people over its economy.

Despite all of this, we can see that overcoming this pandemic will not be an easy task. When interpreting our results, however, several limitations must be considered. Thus, although this is the first study to use a mathematical model to estimate high-risk populations in countries subject to emergencies and quarantine in general and in Italy and Morocco in particular, there are potential limitations with regard to the degree of risk of COVID-19. Where, the degree of risk of developing COVID-19 depends mainly on age, male gender and the presence of comorbidities (obesity, diabetes, heart disease, lung disease and kidney disease) [27], and therefore other results may be assessing the development of COVID-19 in these people. However, we have estimated the prevalence of COVID-19 in these coun-

tries regardless of age, gender and complications. In addition, errors in data collection cause the model to reduce or potentially overestimate future propagation projections. Another limitation is that the authorities frequently change their control strategy by adding some additional controls such as masks commitment, more restrictions on movement ... all of which can lead to massive errors in our prediction, however, our optimal control strategy is still more efficiency even if there are different numbers of the population, and this is verified in this paper by analyzing data of two countries with different initial states.

CONCLUSION

In this paper, we have presented a new mathematical model describing the evolution of the COVID-19 in countries under the nationwide lockdown. In which we have considered two new classes of people. Those who underestimate the quarantine and then left their home for their reasons, we called them the partially controlled people and those who respect the national quarantine by staying at home we called them the totally controlled people. First, we estimated the amount of these populations in Italy and Morocco, by applying a nonlinear least squares method on real data collected and published by the John Hopkins University. In Italy, we found that the number of the partially and totally controlled individuals rose slowly compared to the case of Morocco, this shows the rapid response to quarantine and the efficiency of awareness programs in Morocco. In order to contribute to the control of the COVID-19 in Morocco and Italy and other countries, we have investigated an optimal control problem that aims to reduce the number of partially controlled and infected people with minimal costs. Where this strategy of control we present here adopts the no-medicine control which can be used in all developing countries. We simulated what would have been happened in Italy and Morocco if this strategy of control was applied early. We have provided several simulations throughout the paper to illustrate the efficiency of each part of the manuscript.

COMPETING INTERESTS

The authors have no competing interests to declare.

ACKNOWLEDGMENTS

The authors would like to thank all the members of the Editorial Board who were responsible for this paper.

AUTHOR CONTRIBUTIONS

All authors have contributed equally to the article.

REFERENCES

[1] Rothan HA, Byrareddy SN. The epidemiology and pathogenesis of coronavirus disease (COVID-19) outbreak. Journal of Autoimmunity [Internet]. 2020;109: 102433. Available from: https://doi.org/10.1016/j.jaut.2020.102433

[2] World Health Organization. Health-topics. WHO [Internet]. 2020; Available from: *https://www.who.int/health-topics/*

[3] Weinkove R, McQuilten Z, Blyth E, Cheng AC, Conyers R, Crane M, et al. Managing haematology and oncology patients during the COVID-19 pandemic: Interim consensus guidance. The Medical Journal of Australia [Internet]. 2020;212(10):481-489. Available from: https://doi.org/10.5694/mja2.50607

[4] World Health Organization. Rolling updates on coronavirus disease (COVID-19). WHO [Internet]. 2020; Available from: *https://www.who.int/emergencies/diseases/novel-coronavirus-2019/events-as-they-happen*

[5] Ellyantt H. Italy passes 10,000 coronavirus cases as national quarantine moves closer to total shutdown. CNBC [Internet]. 2020; Available from: *https://www.cnbc.com/2020/03/11/italy-passes-10000-coronavirus-cases.html*

[6] Chen H, Xu W, Paris C, Reeson A, Li X. Social distance and SARS memory: impact on the public awareness of 2019 novel coronavirus (COVID-19) outbreak. medRxiv [Preprint]. 2020. https://doi.org/10.1101/2020.03.11.20033688

[7] Mackay J. Under coronavirus lockdown, Italy is finding a fragile sense of solidarity. The Guardian [Internet]. 2020; Available from: *https://www.theguardian.com/commentisfree/2020/mar/10/coronavirus-lockdown-italy-florence-panic*

[8] ITV News. Panic buying in Italy as nationwide coronavirus lockdown gets underway [Internet]. 2020; Available from: *https://www.itv.com/news/2020-03-09/whole-of-italy-now-subject-to-coronavirus-quarantine-restrictions/*

[9] Zhou W, Wang A, Xia F, Xiao Y, Tang S. Effects of media reporting on mitigating spread of COVID-19 in the early phase of the outbreak. Mathematical Biosciences and Engineering [Internet]. 2020;17(3): 2693-2707. Available from: http://dx.doi.org/10.3934/mbe.2020147

[10] The Center for Systems Science, at Johns Hopkins University (JHU) EC. Novel Coronavirus (COVID-19) Cases [Internet]. 2020; Available from: *https://github.com/CSSEGISandData/COVID-19*

[11] The Center for Systems Science, at Johns Hopkins University (JHU) EC. Coronavirus COVID-19 Global Cases [Internet]. 2020;Available from: *https://www.arcgis.com/apps/opsdashboard/index.html#/bda7594740fd40299423467b48e9ecf6*

[12] DXY. COVID-19 Global pandemic real time report [Internet]. 2020;Available from: *https://ncov.dxy.cn/ncovh5/view/en_pneumonia?from=dxy*

[13] CCDC. COVID-19 Tracking the Epidemic [Internet]. 2020;Available from: *http://weekly.chinacdc.cn/news/TrackingtheEpidemic.htm*

[14] Government of the Hong Kong special administrative region T. COVID-19 Tracking the Epidemic [Internet]. 2020;Available from: *https://www.coronavirus.gov.hk/eng/index.html*

[15] Macau Government. Daily reports for Tracking the Epidemic of COVID-19 [Internet]. 2020;Available from: *https://www.ssm.gov.mo/portal/*

[16] Taiwan CDC. COVID-19 Tracking the Epidemic [Internet]. 2020; Available from: *https://sites.google.com/cdc.gov.tw/2019ncov/taiwan?authuser=0*

[17] European Centre for Disease Prevention and Control. COVID-19 situation update worldwide [Internet]. 2020; Available from: *https://www.ecdc.europa.eu/en/geographical-distribution-2019-ncov-cases*

[18] Pontryagin. Mathematical theory of optimal processes. London: Routledge. 1987. 360p. https://doi.org/10.1201/9780203749319

[19] Sethi SP, Thompson GL. Applications to management science and economics. Boston: Kluwer Academic Publishers. 2000. 524p.

[20] Zakary O, Rachik M, Elmouki I. On the analysis of a multi-regions discrete SIR epidemic model: an optimal control approach. International Journal of Dynamics and Control [Internet]. 2017;5(3):917-930. Available from: https://doi.org/10.1007/s40435-016-0233-2

[21] Zakary O, Rachik M, Elmouki I. A new epidemic modeling approach: Multi-regions discrete-time model with travel-blocking vicinity optimal control strategy. Infectious Disease Modelling [Internet]. 2017;2(3):304-322. Available from: https://doi.org/10.1016/j.idm.2017.06.003

[22] Boutayeb H, Bidah S, Zakary O, Rachik M. A New Simple Epidemic Discrete-Time Model Describing the Dissemination of Information with Optimal Control Strategy. Discrete Dynamics in Nature and Society [Internet]. 2020;2020:7465761. Available from: https://doi.org/10.1155/2020/7465761

[23] Einian M, Tabarraei HR. Modeling of COVID-19 Pandemic and Scenarios for Containment. medRxiv. [Preprint]. 2020. https://doi.org/10.1101/2020.03.27.20045849

[24] Tian J, Wu J, Bao Y, Weng X, Shi L, Liu B, Yu X, Qi L, Liu Z. Modeling analysis of COVID-19 based on morbidity data in Anhui, China. Mathematical Biosciences and Engineering [Internet]. 2020;17(4):2842-52. Available from: http://dx.doi.org/10.3934/mbe.2020158

[25] Kingdom of Morocco Ministry of National Education HE Vocational Training. Press release-March 16, 2020 [Internet]. 2020; Available from: *https://www.men.gov.ma/Ar/Pages/Publication.aspx?IDPublication=5938*

[26] Kingdom of Morocco Ministry of National Education HE Vocational Training. Newsletter no. 3- March 16, 2020 [Internet]. 2020;Available from: *https://www.men.gov.ma/Ar/Pages/Publication.aspx?IDPublication=5941*

[27] D'Antiga L. Coronaviruses and Immunosuppressed Patients: The Facts During the Third Epidemic. Liver Transplantation [Internet]. 2020; 26(6):832-834. Available from: https://doi.org/10.1002/lt.25756

RESEARCH ARTICLE

Vol. 42 | No. 1 | **JANUARY - APRIL 2021** | pp 27-35

REVISTA MEXICANA DE Ingeniería Biomédica

dx.doi.org/10.17488/RMIB.42.1.3

E-LOCATION ID: 1061

A Method for Evaluating the Risk of Exposure to COVID-19 by Using Location Data

Un Método para la Evaluación del Riesgo de Exposición al Virus de COVID-19 Usando los Datos de Locación

Gerardo Mendizabal-Ruiz

Universidad de Guadalajara

ABSTRACT

One of the main reasons for the widespread dissemination of COVID-19 is that many infected people are asymptomatic. Consequently, they likely spread the virus to other people as they continue their everyday life. This emphasizes the importance for targeting high-risk groups for the diagnosis of COVID-19 (with real-time PCR techniques). However, the availability of the necessary technology and resources may be limited in certain towns, cities or countries. Thus, the challenge is to determine a criterion in order to prioritize the suspected cases most in need of testing. The aim of the present study was to develop a method for evaluating the risk of exposure to COVID-19 infection based on geolocation data. The risk is expressed as a score that will be instrumental in optimally applying the COVID-19 test to suspected cases representing the highest probability of exposure. It can be easily and quickly implemented with easily accessible open source tools. A simulation was herein conducted with data from four people, assigning infection to one of them. The results show the feasibility of assessing the risk of exposure with the new methodology. Additionally, the data obtained might provide insights into the sometimes complicated patterns of virus propagation.

KEYWORDS: Risk assessment, COVID-19, location data.

RESUMEN

Una de las principales razones del esparcimiento del COVID-19 es que muchas de las personas infectadas son asintomáticas. Así entonces, al continuar con su vida diaria estas personas contagiadas son susceptibles a contagiar el virus a otras personas sin siquiera imaginarlo. Actualmente el diagnostico de COVID-19 se lleva a cabo usando técnicas de PCR en tiempo real. Sin embargo, la disponibilidad de dichas pruebas puede ser limitada en algunos países o ciudades. En este sentido determinar un criterio que permita definir a cuáles casos sospechosos deben de ser aplicada la prueba resulta un reto importante. En este artículo se presenta un método que permite evaluar el riesgo de exposición de una persona al COVID-19 que está basado en el uso de los datos locación. El método propuesto puede ser rápida y fácilmente implementada utilizando herramientas de código abierto existentes actualmente. El método propuesto fue probado utilizando datos de cuatro personas simulando a uno de ellos como portador del virus. Los resultados muestran la factibilidad del método propuesto para evaluar el riesgo de exposición. Además, los datos que se obtienen pueden ser potencialmente utilizados para un mejor entendimiento de los patrones de dispersión del virus.

KEYWORDS: Evaluación de riesgo, COVID-19, datos de localización.

Corresponding author

TO: Eduardo Gerardo Mendizabal Ruiz
INSTITUTION: Universidad de Guadalajara
ADDRESS: Av. Juárez #976, Col. Centro, C. P. 44100, Guadalajara, Jalisco, México
E-MAIL: gerardo.mendizabal@academicos.udg.mx

Received:

11 May 2020

Accepted:

24 July 2020

INTRODUCTION

COVID-19 is spreading across the world at an alarming rate, making the global outbreak a significant public health problem [1]. One of the main reasons for the large-scale spread of COVID-19 is that an estimated 80% of carriers are asymptomatic or have mild symptoms [2]. Thus, many infected people could unknowingly spread the virus [3] [4]. Since the COVID-19 virus remains on surfaces and in aerosols for many days under certain conditions, people may get infected by touching contaminated objects long after the carrier has departed [5].

Consequently, opportune testing of suspected cases is crucial for clinical management and outbreak control. According to the World Health Organization, the decision to test an individual should be based on clinical (symptoms) and epidemiological factors (contact with a confirmed case) associated with the likelihood of infection [6].

For suspected cases, nucleic acid amplification analysis (RT-PCR) [6] is recommended for COVID-19 testing. In some towns, cities or countries, unfortunately, the resources for such tests may be limited. Therefore, a criterion is needed to determine when to perform a test once the growing number of cases begins to surpass the resources available. Moreover, in the event that people could assure themselves of a high risk of exposure to infection, they would be more prone to self-quarantine even if they are asymptomatic.

The aim of the present study was to develop a method for evaluating the risk of exposure to COVID-19 infection based on geolocation data. The risk is expressed as a score that will be instrumental in optimizing the application of the COVID-19 test to suspected cases representing the highest probability of exposure. To implement the method, a webpage is created for uploading the geolocation data of confirmed COVID-19 cases of the previous days. The geolocation data of a suspected case is then entered into the same webpage in order to calculate an exposure risk score. The latter is computed based on the number of places where one or more confirmed cases and the suspected case were near each other within overlapping periods. A time window after the departure of the confirmed cases is contemplated to reflect the virus survival time.

MATERIALS AND METHODS

Geolocation data

Modern smartphones have a variety of sensors capable of registering the coordinates, accompanied with timestamps, of the routes taken and places visited by the user. Such data could be saved as a JSON file to create a history of geolocation data, considering two attributes of interest (AOI):

- ***location:*** *the latitude and longitude* of a place visited by the user.

- ***duration:*** the length of time spent at a given place calculated from *startTimestampMS* and *endTimestamMs*, corresponding to the arrival and departure times, respectively.

Google location data

Google allows owners of a device (e.g., a smartphone) to request the history of location data at *https://www.google.com/maps/timeline*. The data is sent to the e-mail account of the user in the form of a zip file containing a folder for each year that Google has collected this information. Location data for each month is stored in a JSON file, which contains data for every day of the month in the form of data objects. The *placeVisit* objects register the places where the user stayed for some period of time. From these data-objects, the AOI can be retrieved.

Registering confirmed cases

A person confirmed to be infected with COVID-19 should provide the location data available in a JSON file. Subsequently, an authorized person (most likely a health authority in charge of the system) uploads the file into a web service offering cloud computing services. The web service reads and parses the JSON data corresponding to the AOI of the previous N days by analyzing each placeVisit object in the file. The values are registered into a relational database, storing only the places and times but not the identity of the confirmed case to conserve the confidentiality of the data. Finally, it is possible to make queries by entering data of suspected cases into the web service.

Computing the exposure risk score

The JSON data of a person who wants to evaluate his or her risk of exposure is utilized similarly, extracting all the placeVisit objects within the last M days. The proposed method is based on the hypothesis that a person (suspected case) has a determined risk of COVID-19 infection whenever they were at the same place of a confirmed case in the same time lapse (or within a given time window following the departure of the latter).

Let AT_S, DT_S, AT_C and DT_C be the arrival and departure times of the suspected and confirmed cases, respectively. Examples are illustrated in Figure 1 of suspected cases at high, medium and low risk of exposure, depending on their arrival and departure times to a specific place. If there is an overlap of periods between the suspected and infected cases, a high risk of infection is assigned. When the arrival time of the suspected case is after the departure time of the confirmed case, the virus survival time must be taken into account. In the event that the arrival time is within the window of virus survival on surfaces, a medium risk of infection exists [5]. If the suspected case has a departure time before the arrival of the confirmed case or an arrival time after the virus survival time, it is possible to designate low risk. A Sigmoid function is employed to compute a risk score Rk for each place k of coincidence of a suspected case with a confirmed case within the defined time window, depending on the difference between the arrival time of the suspected case and the departure time of the confirmed case (i.e., $\Delta(AT_S\text{-}DT_C)$):

$$R_k = \begin{cases} \dfrac{1}{1 + exp^{-\lambda}(\mu - \Delta)} & if \;\; AT_s > DT_c \\ 1 & Otherwise \end{cases}$$

Where μ is the value in hours representing the difference between the arrival time of the suspected case and the departure time of the confirmed case that gives a score of 0.5. The real difference (Δ) is subtracted from μ. The parameter λ is a constant that determines the slope of the transient region of the Sigmoid curve, allowing for control over which values of Δ converge to a risk score of 0. As the difference between the departure time of the confirmed case and the arrival time of the suspected case increases, the risk score for the corresponding place will decrease at a rate dependent on the values of λ and μ.

Finally, a total risk score (R) is computed by adding the risk score of all the places where the suspected case and any of the confirmed cases were near according to the following rules:

- The latitude and longitude of the place visited by the suspected case are equal to the latitude and longitude of the place visited by the confirmed case.

- The numerical value of the arrival time of the suspected case is less than that of the departure time of the confirmed case, and the value of the departure time of the suspected case is greater than the arrival time of the confirmed case (examples 1 and 2 in Fig. 1); or the value of the arrival time of the suspected case is greater than the

arrival time of the confirmed case and less than or equal to the departure time of the confirmed case plus a given range ΔT representing the virus survival time (examples 3 and 4 in Fig. 1).

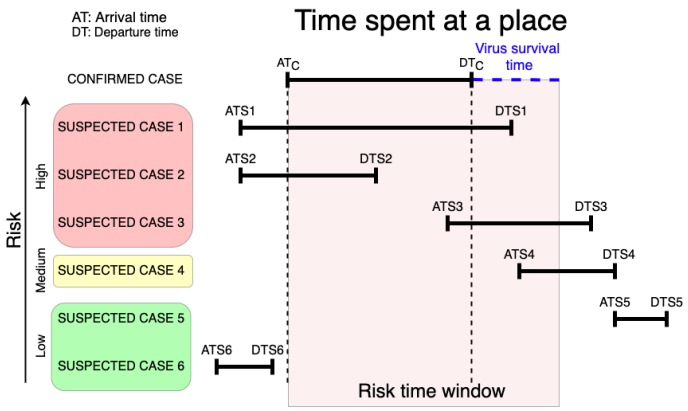

FIGURE 1. Diagram of the risk of infection based on the arrival and departure times of confirmed and suspected cases.

RESULTS AND DISCUSSION

The present method was implemented by using Python 3.7 in the Flask web development framework [7]. The geolocation data employed was extracted from the JSON files downloaded from Google and stored in a MySql database. The places where a suspected case was at risk of exposure are indicated in a map via folium [8]. The system was deployed into a virtual environment by means of Ubuntu 16.04.

The method was evaluated by a simulation based on data from four people (A, B, C and D) during 20 days. The four healthy individuals signed informed consent formats and downloaded the data from the Google Takeout service (*https://takeout.google.com/*). They voluntarily provided the downloaded data for the sake of the simulation.

Persons A, B and C work in the same building but do not necessarily have exactly the same schedule. A and B met in a mall for 3 hours on a particular day. A and D met at a party on one of the days under study. For this exercise, A is assumed to be infected throughout the period being analyzed. For the sigmoid function that determines the exposure risk score during the virus survival time, the values of λ= 0.1 and μ= 12 were adopted. These values were defined to generate a score near 0.5 and 0 when the time elapsed following the departure of the confirmed case was about 12 h and 24 h, respectively.

Risk scores were assigned for each place at which person B was near person A within the time window (Table 1).

TABLE 1. Exposure risk data for person B.

k	AT_c	DT_c	AT_s	DT_s	R_k
1	3/2/20 9:10	3/2/20 13:21	3/2/20 9:09	3/2/20 15:35	1.00
2	3/3/20 8:26	3/3/20 13:31	3/4/20 8:57	3/4/20 16:05	0.32
3	3/4/20 8:27	3/4/20 13:41	3/4/20 8:57	3/4/20 16:05	1.00
4	3/5/20 8:36	3/5/20 11:12	3/5/20 16:37	3/5/20 16:44	0.66
5	3/9/20 8:22	3/9/20 13:19	3/9/20 10:06	3/9/20 10:42	1.00
6	3/9/20 8:22	3/9/20 13:19	3/10/20 10:25	3/10/20 14:38	0.29
7	3/10/20 7:18	3/10/20 12:39	3/10/20 10:25	3/10/20 14:38	1.00
8	3/10/20 7:18	3/10/20 12:39	3/11/20 9:03	3/11/20 14:13	0.30
9	3/11/20 8:24	3/11/20 13:10	3/11/20 9:03	3/11/20 14:13	1.00
10	3/11/20 8:24	3/11/20 13:10	3/12/20 9:18	3/12/20 9:30	0.31
11	3/12/20 7:52	3/12/20 8:57	3/12/20 9:18	3/12/20 9:30	0.76
12	3/12/20 7:52	3/12/20 8:57	3/12/20 14:49	3/12/20 15:07	0.65
13	3/13/20 12:39	3/13/20 13:36	3/13/20 10:19	3/13/20 14:15	1.00
14	3/17/20 12:42	3/17/20 13:48	3/18/20 10:11	3/18/20 10:17	0.30
15	3/19/20 10:11	3/19/20 13:32	3/19/20 9:39	3/19/20 13:34	1.00
16	3/19/20 14:07	3/19/20 14:19	3/19/20 14:08	3/19/20 14:17	1.00
				Risk Score	11.59

In the event that the arrival time of the suspected case was after the departure time of the confirmed case but within the virus survival time, the score is less than one. A map denoting two infection foci

(Figure 2) identifies the places where person B was at risk of exposure (the workplace and the mall). The total risk score for person B is R = 11.59, which is considerably high in the current scheme.

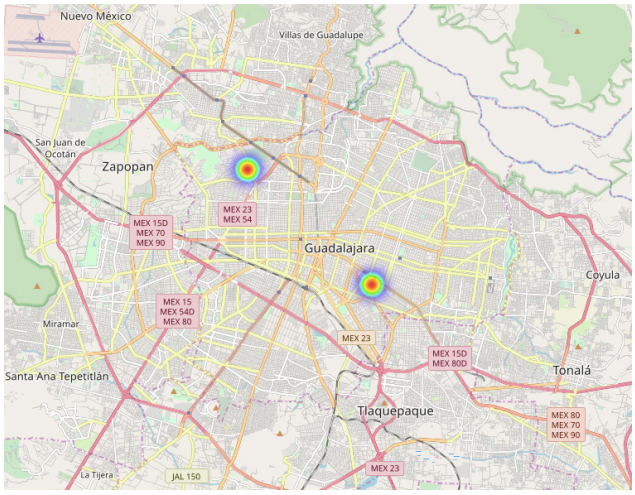

FIGURE 2. **A map highlighting the places where person B was at risk of exposure to infection.**

Risk scores were designated for each place where person C was near person A within the time window (Table 2). As with person B, some of the place scores are less than one (for the aforementioned reason). The first two scores (k=1 and k=2) correspond to the same period for the confirmed case.

TABLE 2. **Exposure risk data for person C.**

k	AT_C	DT_C	AT_S	DT_S	R_k
1	3/2/20 9:10	3/2/20 13:21	3/2/20 7:35	3/2/20 9:20	1.00
2	3/2/20 9:10	3/2/20 13:21	3/2/20 10:50	3/2/20 16:03	1.00
3	3/2/20 9:10	3/2/20 13:21	3/3/20 7:43	3/3/20 9:19	0.35
4	3/3/20 8:26	3/3/20 13:31	3/3/20 7:43	3/3/20 9:19	1.00
5	3/3/20 8:26	3/3/20 13:31	3/4/20 7:48	3/4/20 13:53	0.35
6	3/4/20 8:27	3/4/20 13:41	3/4/20 7:48	3/4/20 13:53	1.00
7	3/4/20 8:27	3/4/20 13:41	3/5/20 7:53	3/5/20 8:44	0.35
8	3/5/20 8:36	3/5/20 11:12	3/5/20 7:53	3/5/20 8:44	1.00
9	3/5/20 8:36	3/5/20 11:12	3/5/20 16:48	3/5/20 16:59	0.65
10	3/6/20 10:42	3/6/20 14:18	3/6/20 16:52	3/6/20 19:14	0.72
11	3/9/20 8:22	3/9/20 13:19	3/9/20 7:53	3/9/20 9:42	1.00
12	3/9/20 8:22	3/9/20 13:19	3/10/20 7:39	3/10/20 8:44	0.35
13	3/10/20 7:18	3/10/20 12:39	3/10/20 7:39	3/10/20 8:44	1.00
14	3/10/20 7:18	3/10/20 12:39	3/11/20 7:37	3/11/20 8:41	0.33
15	3/11/20 8:24	3/11/20 13:10	3/11/20 7:37	3/11/20 8:41	1.00
16	3/11/20 8:24	3/11/20 13:10	3/12/20 7:49	3/12/20 8:48	0.34
17	3/12/20 7:52	3/12/20 8:57	3/12/20 7:49	3/12/20 8:48	1.00
18	3/12/20 7:52	3/12/20 8:57	3/12/20 15:36	3/12/20 19:10	0.63
19	3/13/20 12:39	3/13/20 13:36	3/13/20 15:50	3/13/20 16:42	0.73
				Risk Score	13.79

During that time, person C left the building for some time and came back later. The total risk score is even greater for person C (R = 13.79) than person B.

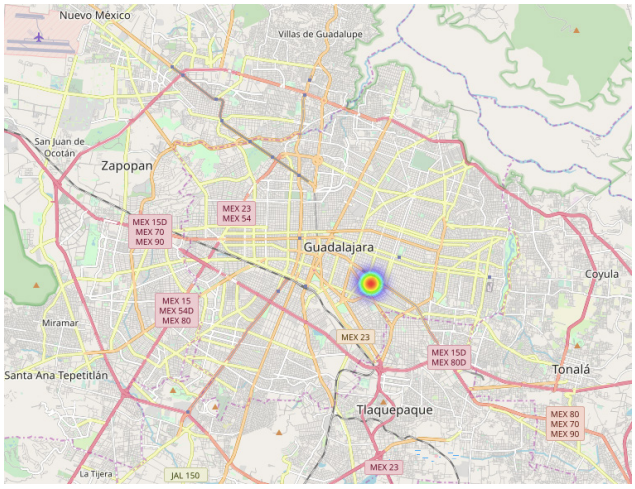

FIGURE 3. **A map portraying the place where person C was at risk of exposure to infection.**

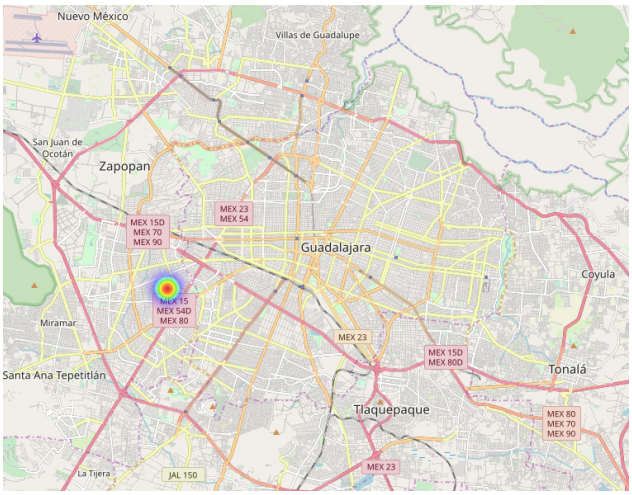

FIGURE 4. **A map depicting the place where person D was at risk of exposure to infection.**

A map is shown with only one place highlighted (the workplace), at which person C was exposed to the risk of infection (Figure 3). A risk score was assigned for a single place and time, representing the occasion person A and person D were at the same party (Table 3).

TABLE 3. Exposure risk data for person D.

k	AT_C	DT_C	AT_S	DT_S	R_k
1	3/12/20 15:14	3/12/20 19:33	3/12/20 15:01	3/12/20 19:16	1
				Risk Score	1.00

The risk score is R = 1 because there was only one occurrence. A map depicts the single place (a party) of the exposure of person D to the risk of infection (Figure 4).

The present results demonstrate that the proposed model can provide reliable exposure risk scores automatically, evidencing the feasibility of its implementation. The computed risk of exposure together with an analysis of the places and circumstances involved (with a risk score >0) may be useful for determining whether a person should be given a PCR-based test. For example, person D has a risk score of 1 due to being in the same place as the confirmed case for only 4 h on one occasion. Thus, he or she is probably not a candidate for testing if asymptomatic, since the time spent at the same place with an infected person was relatively short. However, in the event that person D shows symptoms, he or she is a likely candidate for testing, considering his proximity to a confirmed case. Persons B and C, on the other hand, are good candidates for PCR testing even if they have no symptoms because of sharing the same space with an infected person on repeated occasions for long periods of time.

An obvious limitation of the proposed model is the need for geolocation data. Although this information can be requested from the Google Takeout service, it will probably not be available for all the confirmed and suspected cases. The owner of the mobile device may not have configured a Google account in their mobile device or the location feature might be turned off.

A plausible alternative is the incorporation of a web-based questionnaire or interactive map allowing people to manually enter the locations of places visited and the corresponding times. Nevertheless, the manually entered information has the risk of being less accurate than the data obtained with the Google location files.

Implementation issues

There are two important issues to be considered for the implementation of the current methodology. Firstly, the tracking of user locations records very sensitive data. Secondly, the possibility of entering false information into the system must be confronted. Consequently, the proposed method should be implemented by a central health authority (HA), who could assure the validity of the data entered into the database and the anonymity of the users. The procedure for logging data into the system is illustrated with a flow diagram (Figure 5).

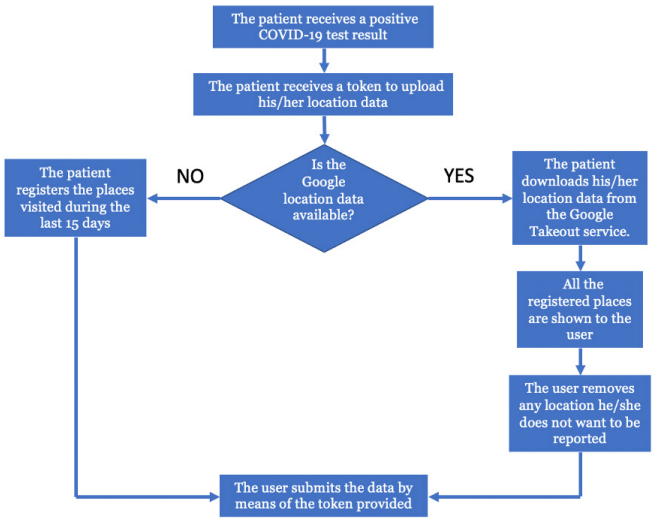

FIGURE 5. A flow diagram of the procedure for logging data into the system.

It is essential to emphasize that the computation of risk scores does not involve any information related to the owner of the device (e.g., smartphone), such as his/her name, age, gender or address. Since public trust in the anonymity of the data collection procedure is crucial, the procedure for registering data must automatically discard any existing confidential information before uploading files to the database.

According to the proposed model, the right to upload data to the system requires a token provided by the HA to the confirmed case at the time he/she receives a positive diagnosis. The token will be generated independently of patient identity information to assure the anonymity of the data. If the confirmed case is connected with the Google Takeout service, he/she can download and review the data. The only factor that could possibly reveal the identity of the owner of the device is the location data itself. Therefore, the data collection procedure has to include an option for the interested party to remove any sensitive location data (e.g., the location of residence). After making any necessary adjustments, the user will upload the data into the system.

CONCLUSIONS

Quarantine and social distancing are recommended measures for helping to contain the epidemic [2]. However, it may be complicated to impose quarantine over long periods of time since the personal and global economy is affected. Hence, a method was herein developed to confront the challenge of controlling the spread of the virus and prioritize COVID-19 testing when resources are limited.

Moreover, the information collected with the proposed procedure could lead to a better understanding of the patterns of dissemination of the virus based on the identification of the most critical places and times involved in infection. This might result in improved models of prediction for use in containing the spread of viruses.

REFERENCES

[1] Lai CC, Shih TP, Ko WC, Tang HJ, Hsueh PR. Severe acute respiratory syndrome coronavirus 2 (SARS-CoV-2) and corona virus disease-2019 (COVID-19): the epidemic and the challenges. International Journal of Antimicrobial Agents. 2020;55(3):105924. https://doi.org/10.1016/j.ijantimicag.2020.105924

[2] Anderson RM, Heesterbeek H, Klinkenberg D, Hollingsworth TD. How will country-based mitigation measures influence the course of the COVID-19 epidemic? The Lancet. 2020;395(10228):931-934. https://doi.org/10.1016/S0140-6736(20)30567-5

[3] Hu Z, Song C, Xu C, Jin G, Chen Y, Xu X, Ma H, Chen W, Lin Y, Zheng Y, Wang J, Hu Z, Yi Y, Shen H. Clinical characteristics of 24 asymptomatic infections with COVID-19 screened among close contacts in Nanjing, China. Science China Life Sciences. 2020;63:706-711. https://doi.org/10.1007/s11427-020-1661-4

[4] Bai Y, Yao L, Wei T, Tian F, Jin DY, Chen L, Wang M. Presumed asymptomatic carrier transmission of COVID-19. JAMA. 2020;323(14):1406-7. https://doi.org/10.1001/jama.2020.2565

[5] van Doremalen N, Bushmaker T, Morris DH, Holbrook MG, Gamble A, Williamson BN, Tamin A, Harcourt JL, Thornburg NJ, Gerber SI, Lloyd-Smith JO. Aerosol and surface stability of SARS-CoV-2 as compared with SARS-CoV-1. New England Journal of Medicine. 2020;382(16) 1564-7. https://doi.org/10.1056/NEJMc2004973

[6] World Health Organization. Laboratory testing for coronavirus disease 2019 (COVID-19) in suspected human cases, interim guidance [Internet]. WHO; 2020. Available from: *https://apps.who.int/iris/handle/10665/331329*

[7] Grinberg M. Flask web development: developing web applications with python. Second Ed. California: O'Reilly Media; 2018. 233p.

[8] Cerquitelli T, Di Corso E, Proto S, Capozzoli A, Bellotti F, Cassese MG, Baralis E, Mellia M, Casagrande S, Tamburini M. Exploring energy performance certificates through visualization. In EDBT/ICDT 2019 Joint Conference. Lisbon: EDBT/ICDT; 2019. https://doi.org/11583/2734573

RESEARCH ARTICLE

Vol. 42 | No. 1 | **JANUARY - APRIL 2021** | pp 36-46

REVISTA MEXICANA DE Ingeniería Biomédica

dx.doi.org/10.17488/RMIB.42.1.4

E-LOCATION ID: 1110

ANOVA to Compare Three Methods to Track COVID-19 in Nine Countries

ANOVA en la comparación de tres métodos para rastrear COVID-19 en nueve países

J. J. Juárez-Lucero[1], A. S. Sánchez-Sánchez[1], R. Díaz-Hernández[1], M. R. Guevara-Villa[2], L. Altamirano-Robles[1]

[1]Instituto Nacional de Astrofísica Óptica y Electrónica

[2]Universidad Politécnica de Puebla

ABSTRACT

A new coronavirus denominated first 2019-nCoV and later SARS-CoV-2 was found in Wuhan, China in December of 2019. This paper compares three mathematical methods: nonlinear regression, SIR, and SEIR epidemic models, to track the covid-19 disease in nine countries affected by the SARS-CoV-2 virus, to help epidemiologists to know the disease trajectory, considering initial data in the pandemic, mainly 100 days from the beginning. To evaluate the results obtained with the three methods one-way ANOVA is applied. The average of predicted infected cases with SARS-CoV-2, obtained with the mentioned methods was: for United States of America 1,098,508, followed by Spain with 226,721, Italy with 202,953, France with 183,897 United Kingdom with 182,190, Germany with 159,407, Canada with 58,696, Mexico with 50,366 and Argentina with 4,860 in average. The one-way ANOVA does not show a significant difference among the results of the projected infected cases by SARS-CoV-2, using nonlinear regression, SIR, and SEIR epidemic methods. The above could mean that initially any method can be used to model the pandemic course.

KEYWORDS: one-way ANOVA; nonlinear regression; SIR; SEIR; COVID-19

RESUMEN

Un nuevo coronavirus denominado primero 2019-nCoV y más tarde SARS-CoV-2 fue encontrado en Wuhan, China en diciembre de 2019. El objetivo de este trabajo es comparar tres métodos matemáticos: regresión no lineal, modelos epidemiológicos SIR y SEIR, para rastrear la enfermedad del COVID-19 en nueve países infectados por el virus SARS-CoV-2, con el propósito de ayudar al epidemiólogo a conocer el curso de la pandemia, considerando principalmente sus primeros 100 días. Para evaluar los resultados obtenidos de la aplicación de los tres métodos, se aplicó ANOVA de una vía. El número promedio de casos infectados con SARS-CoV-2, obtenidos con los tres métodos descritos son: para Estados Unidos 1,098,508, seguido de España con 226,721, Italia con 202,953, Francia con 183,897 Reino Unido con 182,190, Alemania con 159,407, Canadá con 58,696, México con 50,366 y Argentina con 4,860 en promedio. El ANOVA de una vía no muestra diferencias significativas entre los resultados de los casos infectados proyectados por SARS-CoV-2, utilizando la regresión no lineal y los métodos SIR and SEIR. Lo anterior podría señalar que cualquiera de los tres métodos estudiados puede modelar el curso de la pandemia en las condiciones descritas para cada uno.

PALABRAS CLAVE: ANOVA de una vía; regresión no lineal; SIR; SEIR; COVID-19

Corresponding author

TO: **Anabel Socorro Sánchez Sánchez**
INSTITUTION: **Instituto Nacional de Astrofísica Óptica y Electrónica**
ADDRESS: **Luis Enrique Erro #4, Santa María Tonanzintla, C. P. 72840, San Andrés Cholula, Puebla, México**
E-MAIL: **anabel@inaoep.mx**

Received:

20 August 2020

Accepted:

27 November 2020

INTRODUCTION

A new coronavirus denominated first 2019-nCoV and later SARS-CoV-2 was found in Wuhan, China in December of 2019 [1] [2] [3] [4] [5]. This new virus has originated a worldwide pandemic [6], worse than the Severe Acute Respiratory Syndrome Coronavirus epidemic (SARS-CoV) and Middle Eastern Respiratory Syndrome Coronavirus (MERS-CoV) epidemic [7] [8] [9]. It is believed that SARS-CoV-2 jump from the bats to humans, the bats were on the markets and restaurants in Southern China with the potential to cause a global outbreak [10]. The World Health Organization (WHO) called it COVID-19 disease.

Lin *et al*. propose in 2020 a conceptual model to control the COVID-19 outbreak. The model includes among other measurements: holiday extension, travel restriction, hospitalization, and quarantine of the population [11]. Additionally, computational advances in the performance of algorithms may help epidemiologists to take decisions in case of outbreaks [12].

Currently, exist mathematical models to predict or simulate an epidemic spread among them: Nonlinear regression [13], SIR [14], SEIR [15]. Other methods exist that use more variables, but they can be used when the pandemic has already produced enough data it means no at the beginning of the pandemic outbreak.

The Nonlineal model has been used to estimate the impact of the COVID-19 from a global perspective in Germany [13].

The effectiveness of modeling the COVID-19 pandemic with the SIR model was evaluated in 6 countries [14]. And the SEIR epidemic model was employed to build some general control strategies [15]. These three models were chosen because they consider variables that can be known during the epidemic beginning, making it possible to calculate the prediction of the infected people in any country.

The SIR model analyses different variables like the number of people susceptible to sickness, S(t), the number of infected persons, I(t), and the removed people free of spread infection or recovered people, R(t) [16] [17].

The SEIR model uses the same S(t), and R(t), variables adding the exposed time to the disease, E(t), and then studies the effect of infected persons I(t) overexposed people like a new parameter [12] [16] [18] [19] [20] [21]. Meanwhile, if the model includes immunization and population quarantine, Q(t), and isolation, J(t), the SEQIJR model is used [14] [22].

Thus, the aim of this paper to find the first approximation to help epidemiologist taking decisions about pandemic management, mainly at the beginning by comparing three mathematical methods (nonlinear regression, SIR, and SEIR epidemic simulations) used to track the COVID-19 disease in nine representatives countries (Argentina, Canada, France, Germany, Italy, Mexico, Spain, United Kingdom and the United States of America) affected by SARS-CoV-2 virus applying one-way ANOVA.

The nonlinear method was employed as a first statistics approximation and the SIR and SEIR models are based on differential equations solutions taken in account the infected, recovery, susceptible, and dead people.

MATERIALS AND METHODS

Tree mathematical models are applied to simulate COVID-19 disease: Nonlinear regression, SIR, and SEIR. These are described below. Two programs were used from GitHub of MathWorks.

Nonlinear regression model

The nonlinear regression method to obtain the A, B, and C to solve the equation (1), was modeled with Coronavirus Tracker-Country Modeling, available at *https://rb.gy/pbwexu*.

$$y \sim \frac{A}{(1 + C * e^{-Bx})} \quad (1)$$

SIR Model

The SIR model also called Kermack and McKendrick's model was evaluated using the function fitVirus-CV19v3 (COVID-19 SIR Model) from the MathWorks webpage at https://rb.gy/qblldl. This method has three variables or parameters: susceptible (S), infected (I), and recovered (R) [14]. N is the variable that represents the number of total populations in the S(t), I(t), and R(t) functions. This model can be solved by ordinary differential equations solutions with the initial conditions S(0)= S0>0, I(0) = I0>0, R(0)= R0>0. Figure 1 shows the epidemic flow diagram and the equations of the model in (2), (3), (4).

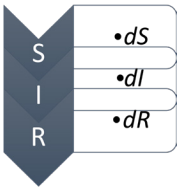

FIGURE 1. Diagram of SIR model following the solutions of the differential equations to find the solution.

$$\frac{dS}{dt} = \frac{-\beta}{N} IS \quad (2)$$

$$\frac{dI}{dt} = \frac{\beta}{N} IS - \gamma I \quad (3)$$

$$\frac{dR}{dt} = \gamma I \quad (4)$$

S(t) is the susceptible, I(t) the infected, and R(t) the recovered people at the time t. β is the constant that represents the contact rate and γ is the inverse of the average infectious period. N is the total population in the function of the other variables

$$N = S(t) + I(t) + R(t) \quad (5)$$

SEIR Model

The SEIR method was modeled with the Epidemic Calculator program obtained from https://rb.gy/4qguan. The SEIR model can analyse infectious diseases where the people have an exposed period to the virus and can transmit the infection to the rest of the population. The epidemic SEIR model diagram is shown in Figure 2 and its equations in (6), (7), (8), (9).

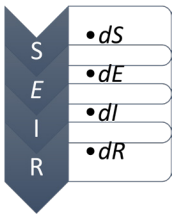

FIGURE 2. Diagram of the SEIR model following the solution of the differential equations to find the solution.

$$\frac{dS}{dt} = -\beta IS \quad (6)$$

$$\frac{dE}{dt} = \frac{\beta}{N} IS - kE \quad (7)$$

$$\frac{dI}{dt} = kE - \gamma I \quad (8)$$

$$\frac{dR}{dt} = -\gamma I \quad (9)$$

S, I, and R are the same values of susceptible, S(t), infected, I(t), and recovery, R(t), people respectively with exposed E(t) in the function of time.

The exposed people E(t) into the SEIR model is constituted by two classes, the first one is related to people that do not have the infection yet, and the second is the persons that change to recovered status. The new population number is:

$$N = S(t) + E(t) + I(t) + R(t) \quad (10)$$

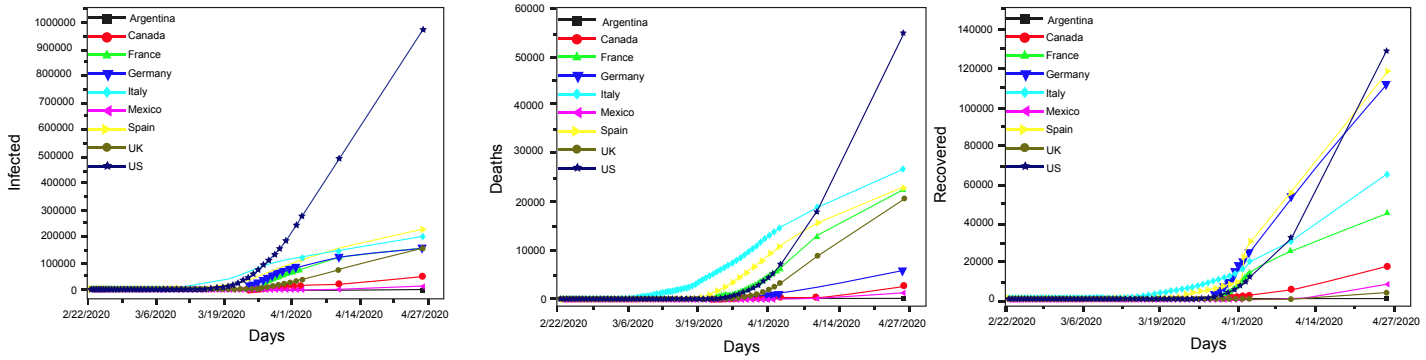

FIGURE 3. Representation of the real number of a) infected, b) deaths, and c) recovered people with the COVID-19 infection from the beginning of the SARS-CoV-2 virus propagation until 4/27/2020 of nine countries in this research.

RESULTS AND DISCUSSION

The nine countries were chosen as a representation from Europe of those where a decrease of SARS-CoV-2 infection was identified. The disease in the early stages in the American continent was evaluated in four of the bigger countries to compare with the European countries. Brazil was discarded because the model SIR cannot be calculated for having many infections peaks. Figure 3 shows the number of real infected, death, and recovered people of COVID-19 disease obtained from *https://data.humdata.org* and *https://covid19info.live/*. These data show that the epidemic is growing, the US has the greatest number of infected people of the nine countries studied followed by Spain, Italy, France, United Kingdom, Germany, Canada, Mexico, and Argentina as shown in figure 3.

In this period Argentina is the country with less infected people. However, the US occupies first place in recovered people followed by Spain, Germany, Italy, France, Canada, Mexico, UK, and Argentina. In the European countries, the disease exists since a few weeks ago and it is just beginning in Latin America. Most deaths were in the US followed by Italy, Spain, France, UK, Germany, Canada, Mexico, and Argentina. To study the propagation of the disease in the countries, one first statistics approximation to predict the maximum of infected cases of COVID-19 disease was realized with the coronavirus tracker, country modeling version 2.6.7 by Joshua McGee from MathWorks. This function was used to evaluate all the variables needed to solve the equations and calculate the values of the A, B, C variables of the equation (1) with the real data obtained from *https://data.humdata.org* of the nine countries studied. The simulation is shown in Figure 4, and the values of the constants A, B, C, and the solutions of the total cases predicted with this model are described in Table 1. The US has a major number of infected people with 1,098,508 sick persons. Argentina on the other hand shows the less sick people with 4,860 predicted confirmed cases.

TABLE 1. Confirmed total cases obtained solving the nonlinear equation 1.

Nonlinear regression simulation[1]				
Country	**A**	**B**	**C**	**Confirmed Total Cases**
Argentina	4,506.9	0.11097	30.922	4,504
Canada	55,765	0.12697	56.777	55,755
France	1.8275e5	0.13328	181.43	182,696
Germany	1.5488e5	0.15681	133.67	154,876
Italy	1.9566e5	0.11976	75.568	195,566
Mexico	44,292	0.10814	170.35	44,140
Spain	2.1922e5	0.14474	54.74	219,213
United Kingdom	1.7088e5	0.14075	252.4	170,846
United States	1.0527e6	0.1384	132.43	1.05256E6

[1] *https://la.mathworks.com/matlabcentral/fileexchange/74557-coronavirus-tracker-country-modeling?s_tid=srchtitle*

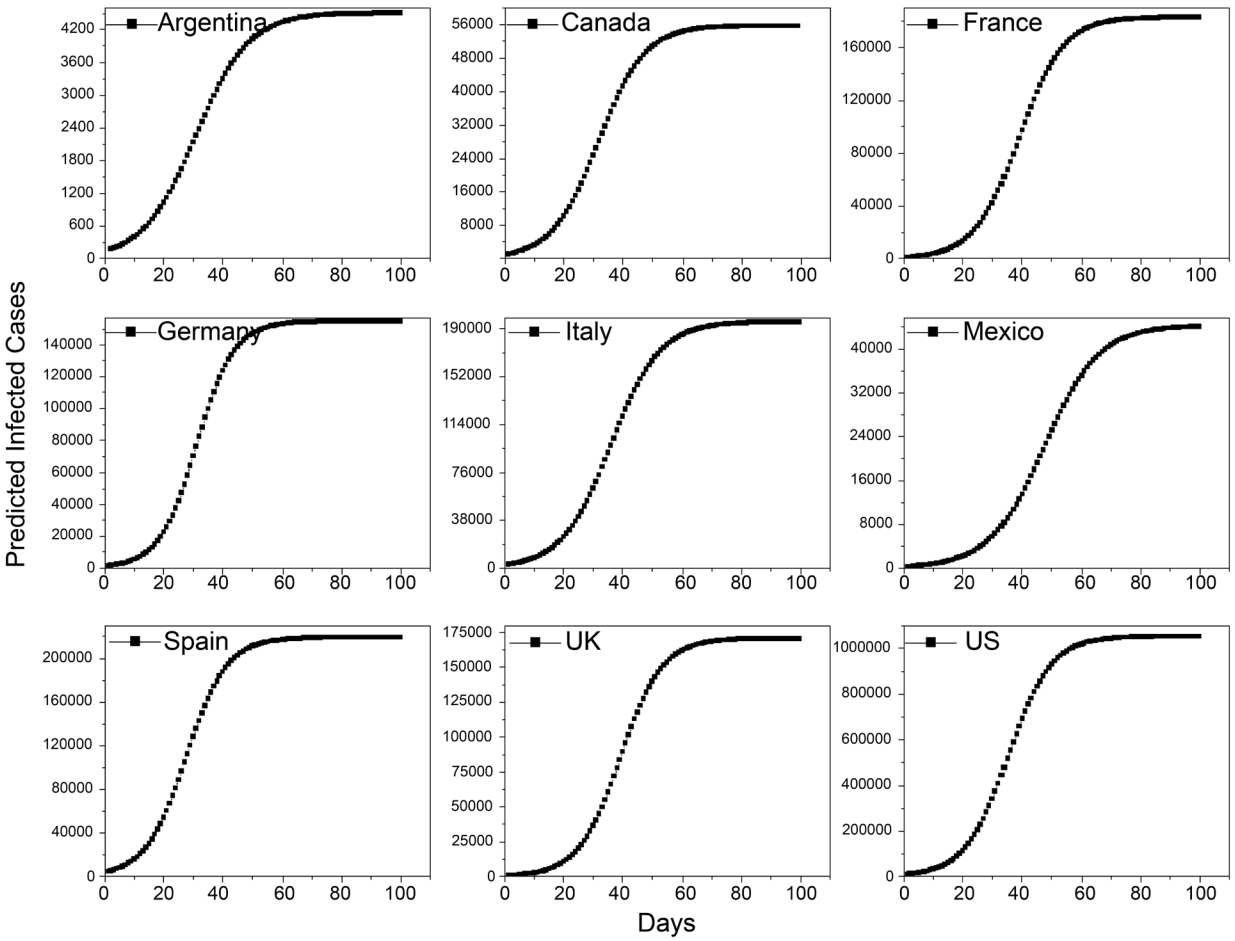

FIGURE 4. The predicted infected cases of SARS-CoV-2 using the nonlinear modelling in Argentina, Canada, France, Germany, Italy, Mexico, Spain, UK and US.

Table 2 shows the projected deaths in the nine countries using the nonlinear regression model. For the US the model predicts the most quantity of deaths with 59,929 followed by Italy with 26,373, France with 25,790, the UK with 23,067, Spain with 22,432, Germany with 5,866, Mexico with 4,077, Canada with 3,148 and for Argentina the model predicts the smallest value with 222.

Results using the SIR epidemic model program downloaded from MathWorks are shown in Figure 5 for each country. The total of daily predicted cases with this model are adjusted for Canada, France, Germany, Italy, Mexico, and the UK, but not for Argentina, Spain, and the US. This model shows that Argentina, Canada,

TABLE 2. Projected deaths using the nonlinear regression simulation.

Nonlinear regression simulation[1]	
Country	**Projected Deaths**
Argentina	222
Canada	3,148
France	25,790
Germany	5,866
Italy	26,373
Mexico	4,077
Spain	22,432
United Kingdom	23,067
United States	59,929

[1] https://la.mathworks.com/matlabcentral/fileexchange/74557-coronavirus-tracker-country-modeling?s_tid=srchtitle

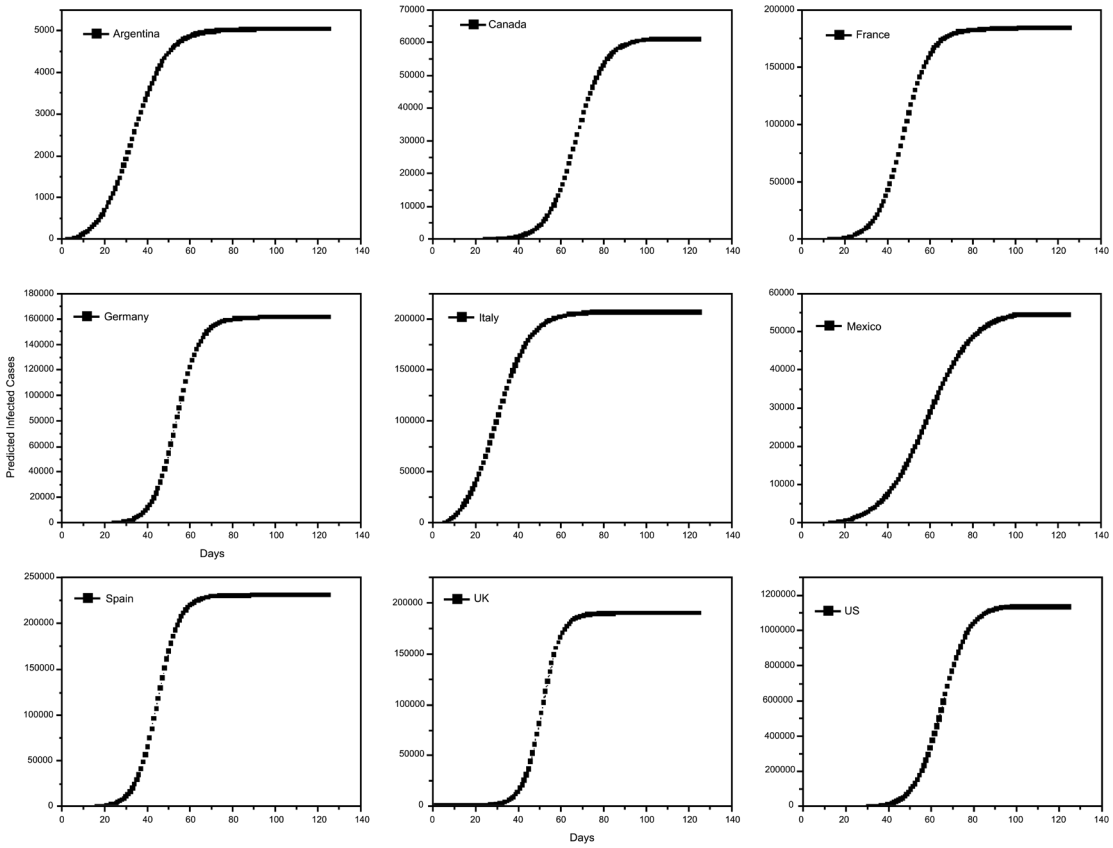

FIGURE 5. The predicted infected cases of SARS-CoV-2 using the SIR epidemic model using fitVirusCV19v3 (COVID-19 SIR Model) by Joshua McGee from MathWorks in a) Argentina, b) Canada, c) France, d) Germany, e) Italy, f) Mexico, g) Spain, h) the UK and i) the US.

France, Germany, Italy, Spain, UK, and the US are decreasing in the number of total daily cases while France, Germany, Italy, and Spain are near to the final cases predicted. Mexico is the only one that is growing the disease. The tendency of cases predicted is near to close in the countries where the COVID-19 started such as France, Germany, Italy, and Spain.

The fitviruscv19v3-covid-19-sir-model function (from MathWorks page, *https://rb.gy/qblldl*) was also used to calculate the values of the contact rate β, the inverse of the average infectious period γ and the basic reproduction number Ro, required to predict the total projected confirmed cases of COVID-19 and these data were used to evaluate both epidemic models (SIR and SEIR). The data obtained from the software are shown in table 3.

TABLE 3. SIR epidemic model simulation values[1].

SIR epidemic model simulation[1]						
Country	**% Deaths[2]**	**% Infected[2]**	**β**	**γ**	**Ro**	**Pop[3]**
Argentina	4.9	66.6	0.641	0.541	1.182	44e6
Canada	5.7	57.5	0.298	0.166	1.792	37e6
France	14	58.1	1.849	1.714	1.079	66e6
Germany	3.9	24	0.307	0.136	2.25	83e6
Italy	13.5	53.1	0.26	0.135	1.928	60e6
Mexico	9.2	32.3	0.239	0.132	1.81	129e6
Spain	10	36	0.29	0.133	2.18	46e6
United Kingdom	13.3	83.9	0.303	0.16	1.896	66e6
United States	5.7	80.5	0.313	0.167	1.868	327e6

[1] *https://la.mathworks.com/matlabcentral/fileexchange/74676-fitviruscv19v3-covid-19-sir-model*
[2] *https://covid19info.live*
[3] *https://www.google.com*

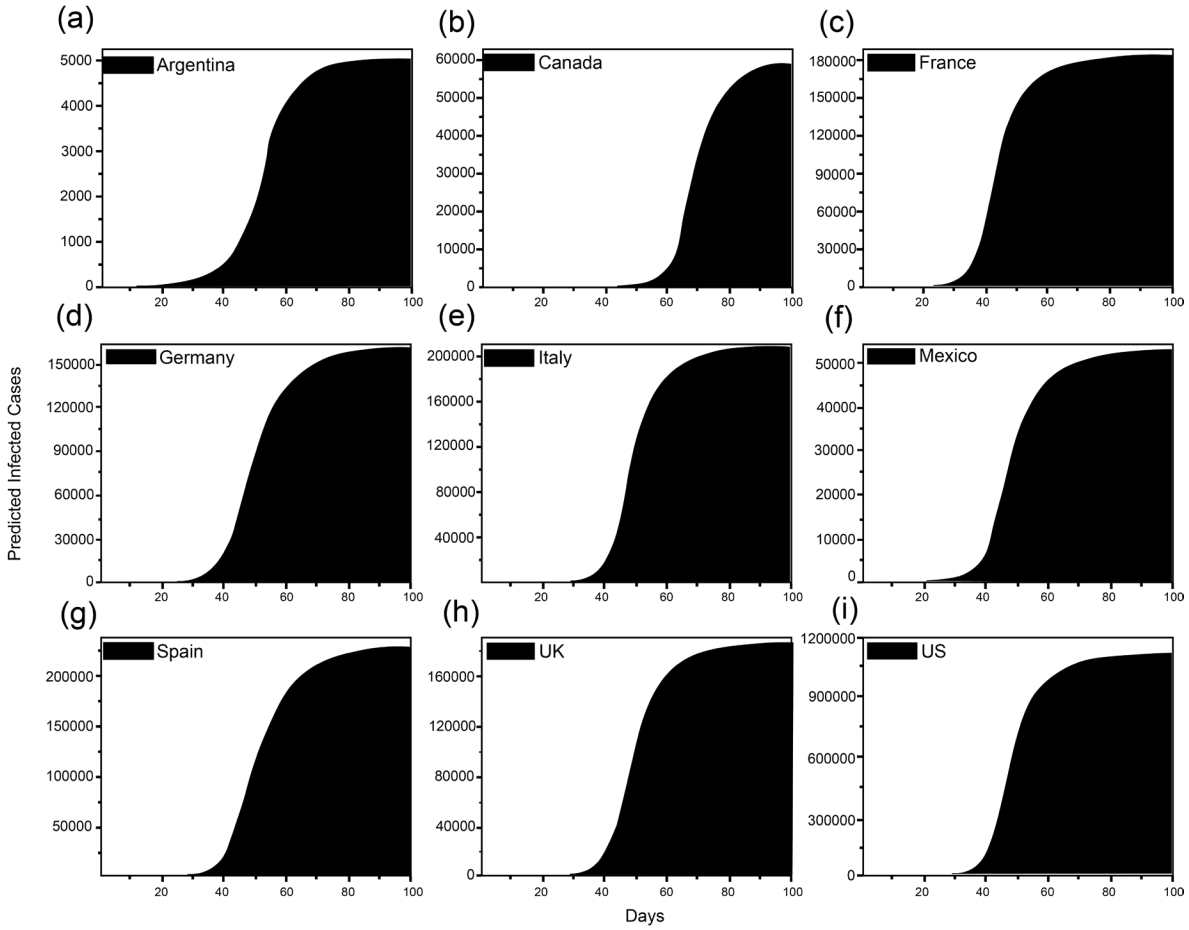

FIGURE 6. The predicted infected cases of SARS-CoV-2 using the SEIR epidemic calculator from the beginning of the COVID-19 infection until 4/27/2020 in a) Argentina, b) Canada, c) France, d) Germany, e) Italy, f) Mexico, g) Spain, h) the UK and i) the US.

The data obtained for β, γ and Ro with the SIR model were used in the simulator of SEIR epidemic model in *http://gabgoh.github.io/COVID/index.html* to obtain the graphs of Figure 6 to predict the projected infected cases in Argentina, Canada, France, Germany, Italy, Mexico, Spain, UK, and the US. Table 4 shows the data of the variables obtained with the SEIR epidemic model to make the predictions.

Table 4 shows values of the contact rate β, the mean exposed period 1/κ, the rate at a recovery of disease γ=1/α, where α represents the infectious period, and basic reproduction number Ro calculated with the SEIR model in the epidemic calculator modeling obtained in *http://gabgoh.github.io/COVID/index.html*.

TABLE 4. SEIR epidemic model simulation[1].

SEIR epidemic model simulation[1]					
Country	**Population**	**Ro**	**B**	**κ**	**α**
Argentina	44e6	1.182	0.22	2.5	0.44
Canada	37e6	1.792	0.21	0.21	0.43
France	66e6	1.079	0.86	6.25	1.72
Germany	83e6	2.25	0.15	0.17	0.29
Italy	60e6	1.928	0.14	0.28	0.29
Mexico	129e6	1.81	0.10	0.45	0.20
Spain	46e6	2.18	0.11	0.25	0.22
United Kingdom	66e6	1.896	0.11	0.41	0.22
United States	327e6	1.868	0.14	0.43	0.29

[1] *http://gabgoh.github.io/COVID/index.html*

Table 5 shows the results predicted using the three models: the nonlinear regression, the SIR and SEIR epidemic model, and the average of the total projected confirmed cases of COVID-19 in the nine studied countries.

TABLE 5. The total confirmed cases of COVID-19 in the nine countries studied.

Total Projected Confirmed Cases				
Country	**Nonlinear regression simulation**	**SIR epidemic model simulation**	**SEIR epidemic model simulation**	**Average**
Argentina	4,504	5,000	5,076	4,860
Canada	55,755	60,053	60,280	58,696
France	182,696	184,286	184,711	183,897
Germany	154,876	161,426	161,921	159,407
Italy	195,566	205,483	207,812	202,953
Mexico	44,140	53,462	53,496	50,366
Spain	219,213	229,050	231,901	226,721
United Kingdom	170,846	187,819	187,905	182,190
United States	1.05256E6	1.12119e6	1,121,774	1,098,508

In figure 7 data are plotted and show that United States has the greatest average number of cases with 1,098,508 followed by Spain with 226,721, Italy with 202,953, France with 183,897 United Kingdom with 182,190, Germany with 159,407, Canada with 58,696, Mexico with 50,366, and Argentina with 4,860 in average.

Like the number of infected people in different countries is not equivalent, the comparison between the three methods is not balanced, besides to find if the methods have a significant difference around the means of nonlinear regression, SIR and SEIR method one-way ANOVA is used to compare them.

One-way ANOVA study is showed in Table 6. As can be seen from the data the three methods mean are not significantly different.

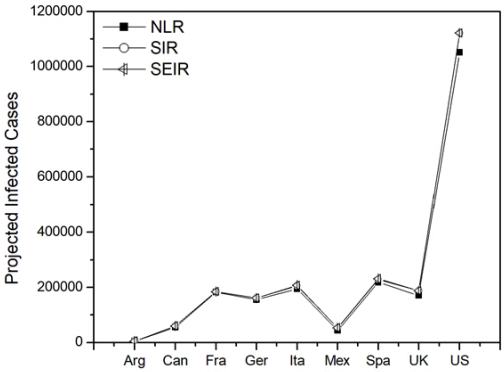

FIGURE 7. Comparison of projected infected cases between the three models studied: nonlinear regression, SIR and SEIR epidemic model of the COVID-19 infection from the beginning of the SARS-CoV-2 virus propagation until 4/27/2020 of nine countries.

Other studies have modeled SARS-COV 2, applying different models including nonlinear regression, SIR, and SEIR epidemic models [7] [11] [12] [13] [14] [15] [18] [19] [20], but they have no compared the results obtained among them as it is done in this paper.

TABLE 6. One-way ANOVA[1] of the nonlinear regression, SIR, and SEIR epidemic model.

One-way ANOVA			
Data	**Mean**	**Variance**	**N**
NLR	231,128.44	1.00629E11	9
SIR	245,307.66	1.13995E11	9
SEIR	246,097.33	1.14054E11	9
F=0.00583			
P=0.99419			

[1]At the 0.05 level

Thus, if the results obtained are considered with the SIR model, then it can be observed that the REAL cases fit very well with the SIMULATED ones. When the SEIR model simulation is carried out, there are no variations, since there is no effect to take into account "for this virus" with the asymptomatic people who were exposed, E (t), since they do not generate significant variations for the model. Then the two models present

similar results, which is what is being obtained in the one-way ANOVA. Therefore, it could be said from this comparison, that the SIR model is sufficient to predict the rest of the pandemic. Additionally, it is possible to see that for the SEIR model, there is a little effect when asymptomatic exposed people to this virus are taken into account, it can be assumed that there is no effect because they are only infecting the others, and since they do not present symptoms, the SEIR model considers them healthy until they are already part of the group of infected, I (t), so the results are similar.

On the other hand, the linear regression model is only making an adjustment with the real data and only allows predicting the maximum value of possible cases of infected people, but the SIR model can predict the daily cases and their decrease per day and predict how long the infection period can last.

CONCLUSIONS

The nine countries studied concerning the projected infected cases by SARS-CoV-2 using nonlinear regression method, SIR and SEIR epidemic model simulation, do no show equal predicted values, but those are not statistically different. It is confirmed by one-way ANOVA analysis. The above could mean that initially any method can be used to model the pandemic course.

These methods can be a first approximation and could help health professionals, not only the epidemiologist, to make decisions with a general point of view of a pandemic evolution.

AUTHOR CONTRIBUTIONS

J.J.J.L. Carried out the analysis, performed calculations for the models and code execution and the ANOVA analysis. Writing the manuscript. A.S.S.S. Conceived the study and wrote the manuscript. Prepared the figures and tables, performed the ANOVA analysis, and carried out conclusions. R.D.H. Caried out analysis and evaluation, performed code execution and calculations for Nonlinear model. M.R.G.G.V. Carried out analysis and evaluation, performed code execution and calculations for SEIR model. L.A.R. Carried out graphics distribution and performed experiments. Supervised writing of manuscript.

REFERENCES

[1] Phan T. Novel coronavirus: From discovery to clinical diagnostics. Infect Gen Evol [Internet]. 2020;79:104210-104211. Available from: https://doi.org/10.1016/j.meegid.2020.104211

[2] Xie M, Chen Q. Insight into 2019 novel coronavirus - an updated intrim review and lessons from SARS-CoV and MERS-CoV. Int J Infect Dis [Internet]. 2020;94:119-124. Available from: https://doi.org/10.1016/j.ijid.2020.03.071

[3] Lupia T, Scabini S, Mornese-Pinna S, Di-Perri G, Giuseppe-De-Rosa F, Corcione S. 2019 novel coronavirus (2019-nCoV) outbreak: A new challenge. J Global Antimicrob Resist. [Internet] 2020;21:22-27. Available from: https://doi.org/10.1016/j.jgar.2020.02.021

[4] Shereen MA, Khan S, Kazmi A, Bashir N, Siddique R. COVID-19 infection: Origin, transmission, and characteristics of human coronaviruses. J Adv Res [Internet]. 2020;24:91-98. Available from: https://doi.org/10.1016/j.jare.2020.03.005

[5] Ghinai I, McPherson TD, Hunter JC, Kirking HL, Christiansen D, Joshi K, et al. First known person-to-person transmission of severe acute respiratory syndrome coronavirus 2 (SARS-CoV-2) in the US. The Lancet [Internet]. 2020;395(10230):1137-1144. Available from: https://doi.org/10.1016/S0140-6736(20)30607-3

[6] Lai CC, Shih TP, Ko WC, Tang HJ, Hsueh PR. Severe acute respiratory syndrome coronavirus 2 (SARS-CoV-2) and coronavirus disease-2019 (COVID-19): The epidemic and the challenges. Int J Antimicrob Agents [Internet]. 2020;55(3):105924. Available from: https://doi.org/10.1016/j.ijantimicag.2020.105924

[7] Luk HKH, Li X, Fung J, Lau SPK, Woo PCY. Molecular epidemiology, evolution, and phylogeny of SARS coronavirus. Infect Genet Evol [Internet]. 2019;71(Jul):21-30. Available from: https://doi.org/10.1016/j.meegid.2019.03.001

[8] Ramadan N, Shaib H. Middle East respiratory syndrome coronavirus (MERS-CoV): A review. Germs [Internet]. 2019;9(1):35-42. Available from: https://dx.doi.org/10.18683%2Fgerms.2019.1155

[9] Law S, Leung AW, Xu C. Severe Acute Respiratory Syndrome (SARS) and Coronavirus disease-2019 (COVID-19): From Causes to Preventions in Hong Kong. Int J Infect Dis [Internet]. 2020;94:156-163. Available from: https://doi.org/10.1016/j.ijid.2020.03.059

[10] Wong ACP, Li X, Lau SKP, Woo PC. Global Epidemiology of Bat Coronaviruses. Viruses [Internet]. 2019; 11(2):174. Available from: https://doi.org/10.3390/v11020174

[11] Lin Q, Zhao S, Gao D, Lou Y, Yang S, Musa SS, He D. A conceptual model for the coronavirus disease 2019 (COVID-19) outbreak in Wuhan, China with individual reaction and governmental action. Int J Infect Dis [Internet]. 2020; 93:211-216. Available from: https://doi.org/10.1016/j.ijid.2020.02.058

[12] Shatnawi M, Lazarova-Molnar S, Zaki N. Modeling and simulation of epidemic spread: Recent advances. In: 9th International Conference on Innovations in Information Technology (IIT) [Internet]. Abu Dhabi: IEEE; 2013:118-123. Available from: https://doi.org/10.1109/Innovations.2013.6544404

[13] Ershkov SV, Christianto V, Rachinskaya A., Prosviryakov EY. A nonlinear heuristic model for estimation of Covid-19 impact to world. Roma Rep Phys [Internet]. 2020;72:1-16. Available from: *http://www.rrp.infim.ro/2020/AN72605.pdf*

[14] Cooper I, Mondal A, Antonopoulos CG. A SIR model assumption for the spread of COVID-19 in different communities. Chaos Soliton Fract [Internet]. 2020; 139:110057. Available form: https://doi.org/10.1016/j.chaos.2020.110057

[15] He S, Peng Y, Sun K. SEIR modeling of the COVID-19 and its dynamics. Nonlinear Dyn [Internet]. 2020; 101:1667-1680. Available from: https://doi.org/10.1007/s11071-020-05743-y

[16] Brauer F, Castillo-Chávez C. Discrete population models. In: Mathematical models in population biology and epidemiology [Internet]. New York: Springer; 2001. 51-94p. Available from: https://doi.org/10.1007/978-1-4757-3516-1_2

[17] Agrawal A, Tenguria A, Modi G. MATLAB Programming for Simulation of an SIR Deterministic Epidemic Model. IJMTT [Internet]. 2017;50(1):71-73. Available from: https://doi.org/10.14445/22315373/IJMTT-V50P509

[18] Al-Sheikh SA. Modeling and Analysis of an SEIR Epidemic Model with a Limited Resource for Treatment. GJSFR Mathematics and Decision Sciences [Internet]. 2012; 12(14):56-66. Available from: *https://globaljournals.org/GJSFR_Volume12/5-Modeling-and-Analysis-of-an-SEIR-Epidemic.pdf*

[19] Agrawal A, Tenguria A, Modi G. Global analysis of an SEIRS epidemic model with saturated incidence and saturated treatment. AJOMCOR [Internet]. 2017;22(2):43-56. Available from: *https://www.ikprress.org/index.php/AJOMCOR/article/view/1150*

[20] Yan P, Liu S. SEIR epidemic model with delay. ANZIAM J [Internet]. 2006;48(1):119-134. Available from: https://doi.org/10.1017/S144618110000345X

[21] Stehlé J, Voirin N, Barrat A, Cattuto C, Colizza V, Isella L, Vanhems P. Simulation of an SEIR infectious disease model on the dynamic contact network of conference attendees. BMC Med [Internet]. 2011;9:87. Available from: https://doi.org/10.1186/1741-7015-9-87

[22] Siriprapaiwan S, Moore EJ, Koonprasert S. Generalized reproduction numbers, sensitivity analysis and critical immunity levels of an SEQIJR disease model with immunization and varying total population size. Math Comput Simul [Internet]. 2018;146:70-89. Available from: https://doi.org/10.1016/j.matcom.2017.10.006

[23] McGee J. MathWorks. Coronavirus Tracker - Country Modeling [Internet]. 2020; Available from: *https://github.com/joshmcgee24/coronavirustracker*

RESEARCH ARTICLE

Vol. 42 | No. 1 | **JANUARY - APRIL 2021** | pp 47-62

REVISTA MEXICANA DE Ingeniería Biomédica

dx.doi.org/10.17488/RMIB.42.1.5

E-LOCATION ID: **1115**

Implementation and Technical Testing of a Robot for Future Use in Patients Care (Covid-19)

Implementación y Pruebas Técnicas de un Robot para Uso Futuro en la Atención Hospitalaria (Covid-19)

E. M. Rico-Mesa[1], J. G. Barrientos-Gómez[2], S. Correa-Zapata[1], V. A. Acevedo-Urrego[2], P. A. Palacios-Correa[1], V. A. Álvarez-Tobón[2], J. C. Londoño-Lopera[1], Y. A. Aguilar-Pérez[2], Y. S. Jaramillo-Munera[1], E. A. Torres-Silva[2], C. A. Vergara-Crismatt[1], B. S. Jiménez-Franco[2], L. Tobón-Ospina[1], J. S. Parada-Zuluaga[2], J. E. Goez-Mora[1], J. S. Tamayo-Zapata[1], J. D. Arismendy-Pulgarín[1]

[1]Servicio Nacional de Aprendizaje de Colombia SENA

[2]Clínica Universitaria Bolivariana

ABSTRACT

The present paper describes a mobile robot's construction with telemedicine functions built by a multi-disciplinary team of engineers and doctors. During this process, a technical test was applied to the Robot, employing medical care simulations. The technical test was carried out in a hospital in Medellín - Colombia, which verifies the robot behaviors in its displacement, stability, and temperature measurement. The hospital environment's robot viability has been studied, presenting the positive and negative aspects through a Strengths, Weaknesses, Opportunities, and Threats (SWOT) analysis matrix and its targeting through action strategies. In the future, the robotic system will work in health institutions to accompany patients and professionals in the crisis caused by the *SARS-CoV-2* virus (COVID-19).

KEYWORDS: Medical assistant robot; Telemedicine; Technical evaluation; *SARS-CoV-2*; SWOT Matrix

RESUMEN

El presente artículo describe la construcción de un robot móvil con funciones de telemedicina construida por un equipo multidisciplinario de ingenieros y médicos. Durante este proceso, se aplicó una prueba técnica al Robot, empleando simulaciones de atención médica. La prueba técnica, que consistió en verificar los comportamientos del robot en su desplazamiento, estabilidad y medición de temperatura, se realizó en un hospital de Medellín - Colombia. Se ha estudiado la viabilidad del robot en el entorno hospitalario, presentando los aspectos positivos y negativos a través de una matriz de análisis de Fortalezas, Debilidades, Oportunidades y Amenazas (FODA) y su focalización a través de estrategias de acción. En el futuro, el robot trabajará en instituciones de salud para acompañar a pacientes y profesionales en la crisis provocada por el virus *SARS-CoV-2* (COVID-19).

PALABRAS CLAVE: Robot asistente médico; Telemedicina;Evaluación técnica; *SARS-CoV-2*;Matriz FODA

Corresponding author

TO: Edgar Mario Rico Mesa

INSTITUTION: Servicio Nacional de Aprendizaje de Colombia SENA

ADDRESS: Calle 57 #8-69, Barrio Chapinero Central, C. P. 110231, Bogotá, Cundinamarca, Colombia

E-MAIL: emrico@sena.edu.co

Received:

19 September 2021

Accepted:

18 March 2021

INTRODUCTION

In the latest months of 2019 was known about an infectious disease, which is a consequence of the *SARS-CoV-2* virus. This disease was detected in Wuhan's (China) city and caused great concern in both the scientific community and the World Health Organization (WHO). The virus spread rapidly throughout the world, so, on March 11, 2020, the world health organization (WHO) declared the disease associated with this virus as a pandemic [1] [2]. In the actual context, a huge portion of the world population has been confined; the most affected countries are the USA, China, and Italy; nevertheless, as of this article's writing, Latin America is projected as the new epicenter of the pandemic [3]. Several companies and research groups have converged on finding solutions for the health sector to mitigate the crisis. The absence of medical equipment and supplies is currently projected as the main problem affecting the countries fighting against Covid-19 [4]. The first line of care is composed of doctors and internists. Those people are at a high level of exposure to the virus, and they must ensure the least possible interaction with infected patients. Considering the above, the adaptation of technological tools that support basic care processes, such as anamnesis, is essential. The proposed solutions must have a good cost-benefit ratio for the health sector, knowing that it must allocate a few resources to the crisis attention. The number of infected health staff is increasing. This reflects the difficulties in prevention, even when biosecurity standards are implemented. Long working days can generate skin injuries from the continuous use of protective elements [5], which could cause physicians to make mistakes unintentionally in handling their protection. Infections among health staff have critical consequences for the health system since the hospitals and clinics' response capacity is considerably reduced when their personnel is in confinement, as has occurred in China and Italy [6]. Considering the above, robotic systems' contribution is important as tools for health staff to perform specific functions that minimize the risk of infection [7] [8]. Several databases were consulted (Scopus, IEEE, Science Direct, etc.) to find jobs related to remote medical assistance, which are being used in the current *SARS-CoV-2* virus pandemic. Francesco *et al.* [9] presented multi-agent architecture. It is directed to intelligent medical care and can select patients supervised by the doctor on duty. Geng *et al.* [10] implemented a telerobotic system for remote care in patient isolation rooms; the robot plays two roles in the interaction with patients: teleoperation and telepresence. Koppu *et al.* [11] proposed a model of early detection of the disease using a predictive model based on deep learning. This paper describes the implementation of a mobile robot operated by a health institution's medical staff to perform specific telemedicine functions; in this process, a follow up of the hospital attention during the COVID 19 pandemic is made. The paper is organized as follows methods and materials, results and discussion, conclusions, and ethical statement.

MATERIALS AND METHODS

The robotic system was developed according to the needs of "Clínica Universitaria Bolivariana (CUB)" which also addresses some general problems in the health sector. In March 2020, the most suitable materials, electrical, electronic, and mechanical components were selected from "Servicio Nacional de Aprendizaje (SENA)" and the Colombian national market. As for the methodology used, this is an experimental applied research project. Figure 1 shows the methodological framework followed in the development of this project.

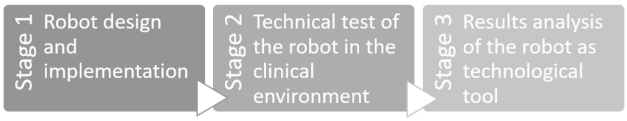

FIGURE 1. Methodological framework.

Stage 1: Robot design and implementation

In April 2020, a robotic system was designed and implemented for remote medical care (telemedicine). The criteria for the operation of the robot was proposed by "Bolivarian University Clinic (CUB)." For this

reason, GACIPE (Research Group in Automation, Industrial Communications, Pedagogy and Alternative Energies) -a SENA's research group-, conceived a system composed of a mobile robot controlled by a "Raspberry Pi 4" board and control system using a graphic user interface implemented on a laptop, based on the following criteria:

- *The materials and the structure must contribute to asepsis and sterilization:*

  The robot's structural cover, support design and construction took the asepsis and sterilization conditions into account. Therefore, a design in the Solid works software was made and this was implemented in 3D printers, whose fundamental characteristic is surfaced flat and smooth curves without any abrupt relief. This type of design intends to facilitate cleaning. The PLA material was chosen because it allows making quick prototyping parts. The mechanical (acceptable tensile strength and modulus of elasticity), physical (adequate resistance to moisture and grease, and good electrical and thermal insulator) properties [12] are suitable for the function that the robot fulfills. The body is developed in aluminum to avoid some oxidation using CNC machines in its implementation.

- *Access confined spaces like regular hospital rooms:*

  In the mechanical design of the structure, the minimum dimension of the robot of 130x40x40 cm was determined, taking into account the ease of moving in confined spaces. Also, the distribution of the weights of the different components and modules of the robot were defined to have stability in movement and avoid probabilities of overturning according to the zero moment point criterion. Simulations evaluated the robot structure in the NX software.

  The robot's electrical and electronic mechanism's design and development use a kinematic model of mobile robotics for four Omnidirectional wheels. This model was designed and implemented to allow stable locomotion of the robot to overcome obstacles in reduced space. For the robot's motion control (kinematics), the controller is a "Raspberry pi 4".

- *Communicate the patient with the doctor and family remotely:*

  In the design and development of the interactive module of the robot, the Ubuntu 18.04 operative system was implemented on the robot's development board ("Raspberry pi 4") and the controller (laptop) in which communication is incorporated by the network (WiFi) to establish remote communication using the high-performance free software video call application called Jitsi Meet as interaction platform.

- *Measure vital signs of the patient and show them online to the doctor:*

  The module selected for the body temperature measurement, the GY906 module, has the MLX90614 sensor. The data obtained by the module are processed and sent via WiFi from the robot to the graphical interface for the doctor to see them online. The set-up and calibration of the temperature for its processing in the robot (carried out by "Raspberry pi 4") was obtained based on the commercial product MCH-370.

- *The quality of the audiovisual system must be of high definition:*

  In the interactive module, the components of the audiovisual system used to execute high definition video calls were defined, consisting of

the high-performance (720p) webcam (image and audio for the doctor) and a high resolution (1080p) capacitive touch of 13.3 inches (Image and audio for the patient).

Once all the criteria proposed by the Bolivarian University Clinic were met, the assembly and tuning of the robot's operation in the clinic was carried out. Therefore, when the robot was complete, a series of functional tests were carried out, in terms of movement in confined spaces, communication between patient and doctor, and verification of vital signs data obtained from patients and battery data to verify the robot's energy autonomy.

Stage 2: Technical test of the robot in the clinical environment

In May 2020, the operation of the robot started in the hospital's facilities. At this time, the design of the intervention plan of the robot in the CUB is determined. In principle, training sessions were held with the clinic's medical staff with the team's accompaniment who developed the robot. This activity aims to appropriate the technological tool and know the doctors' and nurses' perceptions about the robot's advantages and disadvantages. Once this process has been completed, a technical test of equipment operation in clinical service without patients was carried out. This to a medical assistance simulation (pilot test) corresponds to verify aspects of the technological tool's use and handling. During this test, the technical team worked with medical staff and identified barriers and limitations that should be corrected to facilitate future interaction with patients.

Stage3: Results analysis of the robot as a technological tool

In June 2020, a report about the technical performance was made, which describes the health staff's perceptions. The report was focused on analyzing the response of the robotic system as a tool to support patient care. The prototype was technically verified and analyzed from a SWOT matrix, taking into account the pilot test. The elements that should be verified in an eventual usability test with patients in a high complexity health institution were identified.

RESULTS AND DISCUSSION

Results

The project has three main phases in which the transition from the robot to the clinical application is focused.

Robotic system implementation: The robot's development began with meetings among the GACIPE group and the CUB to determine its functions. The defined function is related to telemedicine; the main function was to communicate the health staff and the family with COVID patients. The robot's role established the design, modeling, and construction of the robot's structure and body. The chassis and supports were made of aluminum to avoid oxidation generated by the hospital environment and disinfection procedures (Figure 2A). The bodywork was made of PLA material to make the robot's cleaning easier (Figure 2B) to have a strict aseptic procedure. Also, the robot's weight was an important factor to facilitate its maneuverability within the clinical environment. These aspects were taken into account for the robot's mechanical component (see Figure 2C). The electrical, electronic, and telecommunication modules are developed, considering the mobile robot's conditions and function in the clinic. The motors and wheels have been selected according to the robot's projected weight (25kg) and the surface type for its displacement. The power system is considered according to the technical characteristics of the motors (60w). The batteries are selected according to the autonomy required in the clinic (at least

8 hours). The communication established for audio and video (interactive module) is used through Wi-Fi. However, the transmission of measurement and control data is implemented through radiofrequency (RF). The displacement control, monitoring of variables, and transmission of the video call are developed through a high-performance processing system called "Raspberry pi 4".

a) b) c)

FIGURE 2. Implementation of the body, chassis and structure of the robot. A) Design and construction of the robot chassis. B) Design and development of the robot body. C) Complete mechanical conformation.

The general description of the operation for the system is presented in Figure 3.

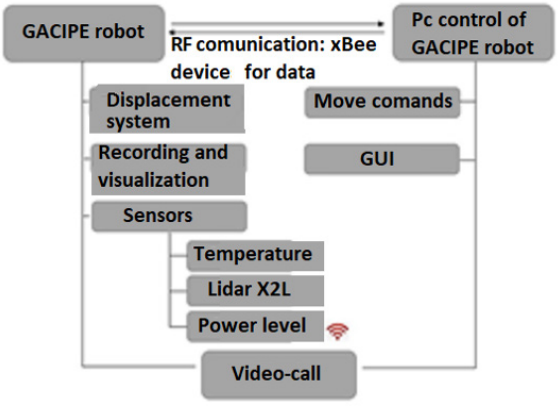

FIGURE 3. Robot processing operating scheme.

Design elements required for robot testing:

- *Kinematics of robot movement:*

The medical assistant robot was designed with omnidirectional wheels, which provide great flexibility in the load movement's movements. It is also very versatile in small spaces. Due to its shape, the kinematic study is more complex. The configuration of the robot can be seen on its own platform in Figure 4.

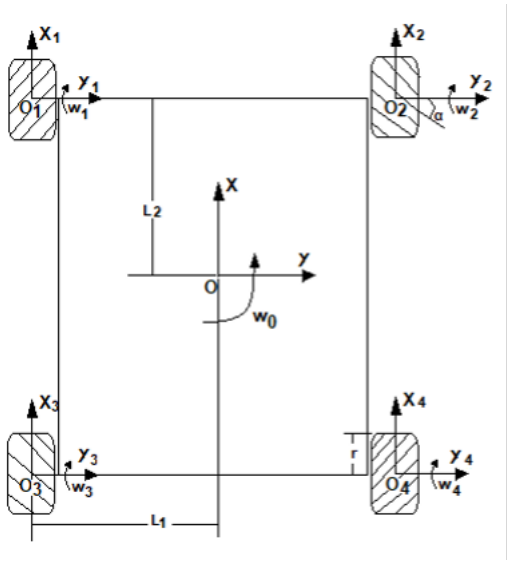

FIGURE 4. Platform top view.

The goal is to know the speed of each tire in terms of linear speeds [13]. It is established:

$$v_w = [w_1 \ w_2 \ w_3 \ w_4]^T \quad (1)$$

$$v_o = [v_x \ v_y \ w_o]^T \quad (2)$$

Where:

w1, w2, w3, w4 corresponds to the angular velocity value of each wheel.

v_x v_y w_o are the velocity in the x, z, axis, and angular velocity around the robot's O point.

From the kinematic analysis [14], it is obtained that:

$$v_w = J(\alpha)v_o \tag{3}$$

With:

α is the angle that determines the direction of each of the rollers to the horizontal.

$$J(\alpha) = \frac{1}{r}\begin{bmatrix} 1 & \frac{1}{\tan\alpha} & -\frac{L_1\tan\alpha + L_2}{\tan\alpha} \\ 1 & -\frac{1}{\tan\alpha} & \frac{L_1\tan\alpha + L_2}{\tan\alpha} \\ 1 & \frac{1}{\tan\alpha} & -\frac{L_1\tan\alpha + L_2}{\tan\alpha} \\ 1 & -\frac{1}{\tan\alpha} & \frac{L_1\tan\alpha + L_2}{\tan\alpha} \end{bmatrix} \tag{4}$$

Being:

r the radius of the wheel.

In this way, it is possible to manipulate the dynamics of the robot's movement [15].

- *Temperature sensor calibration:*

The GY906 module that comes with the MLX90614 sensor signal conditioning is a sensor which measures temperature without contact with objects; it is suitable for medical applications since its measurement error in the range 36-39 degrees Celsius is ± 0.1 degrees centigrade, allowing to obtain relevant measurements on the human body. The calculation of the measurement is configured according to the technical data sheet of the MLX90614. Afterwards, the sensor was compared with a commercial IR temperature measurement product called MCH-370 (TR), whose function is to measure the head's front (product endorsed by "Instituto Nacional de Vigilancia de Medicamentos y Alimentos" - INVIMA - Colombia). For the GY906 (TD) calibration, a series of measurements between 1 and 3 centimeters were made, taking the commercial product as a reference. For this, 5 measurements every 1 cm were taken; the results are presented in terms of error (TR-TD) and distance (see Figure 5).

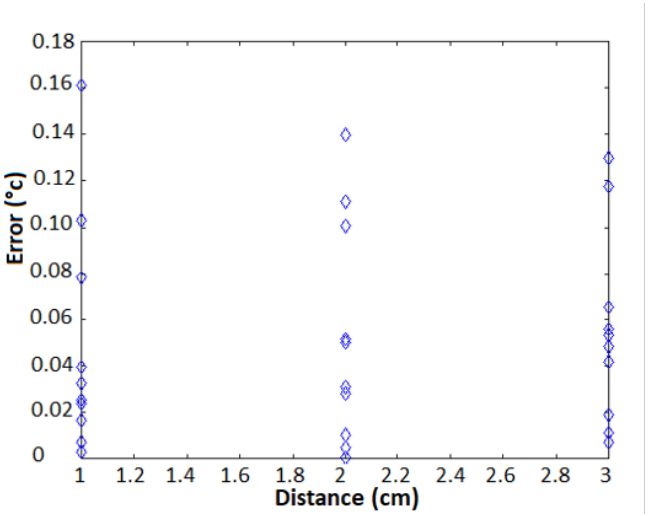

FIGURE 5. Graphic representation of the temperature error from the frontal area of the head measured by GY906.

In these tests, an adequate response has been found for the GY906 module, observing the measurement error in most data below 0.1 degrees centigrade.

- *Robot control:*

Additionally, to control the movement of the robot, the balance of the robot was taken into account at all times based on the criterion of the zero moment point (ZMP) raised by Vukobratovic exposed in articulated robots [16] [17] and mobile robots [18] [19], it is calculated for each point of support (wheel), the center of mass, rotational moment of inertia, angular acceleration, acceleration in the three coordinate axes, taking into account that each wheel has an independent actuator (motor). The x, y coordinate is found

with these data, and with equations 5 and 6 that correspond to the zero-moment point (ZMP) shown in Figure 6. If the coordinates provided are within the polygon armed by the support points, then the system is stable, and the probability of overturning is minimal.

$$x_{ZMP} = (\sum_{i=1}^{n} m_i(\ddot{z}_i + g)\, x_i - \sum_{i=1}^{n}(\ddot{\Omega}_{iy} I_{iy})) / \sum_{i=1}^{n} m_i(\ddot{z}_i + g) \quad (5)$$

$$y_{ZMP} = (\sum_{i=1}^{n} m_i(\ddot{z}_i + g)\, y_i - \sum_{i=1}^{n}(\ddot{\Omega}_{ix} I_{ix})) / \sum_{i=1}^{n} m_i(\ddot{z}_i + g) \quad (6)$$

such that

x_i, y_i, z_i are the coordinates of the Center of Mass (CoM) of each wheel

$\ddot{x}_i$, $\ddot{y}_i$, $\ddot{z}_i$ is the acceleration of the robotic system in z, y, x

$\ddot{\Omega}_i$ is the angular acceleration

I_i is the rotational inertia

g is the acceleration of gravity

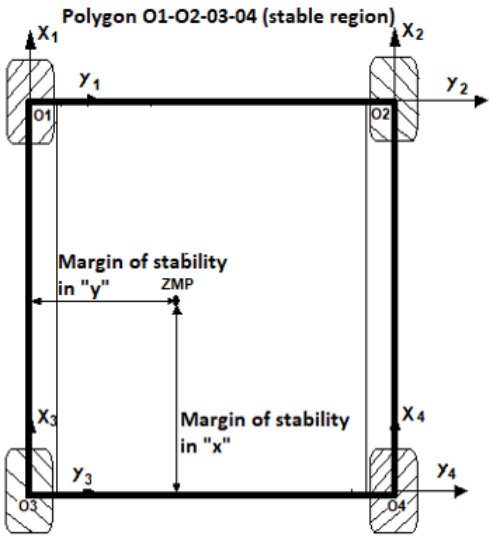

FIGURE 6. **Robot balance.**

- *Robot simulation:*

The robot was configured in Solidworks software and simulated in NX based on the design criteria in kinematics and stability. The test used focuses on the robot, starting from rest moving forward a distance of approximately 1 meter, and ending up again at rest. The robot's simulation environment moving on a flat surface is presented below (see Figure 7).

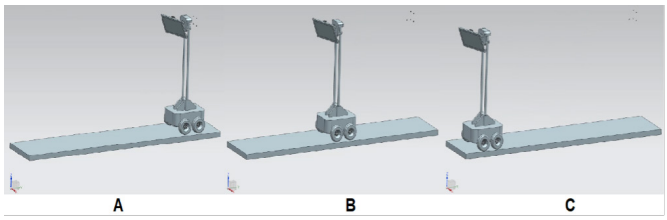

FIGURE 7. **Reproduction of the robot movement in software. A) At the beginning of the road. B) In the middle of the road. C) At the end of the road.**

According to Figure 7, the robot is in a virtual environment moving forward on a flat surface shown through three moments (beginning, middle, and end). In this case, we wanted to analyze the behavior of the robot in its kinematics and stability.

Starting from the case shown in Figure 7B, theoretical and simulated stability and kinematic analysis are carried out, the results of which are established in table 1, taking into account that α= 45 °, v_x prom= 0.377 meters/second, r= 0.075 meters.

According to Table 1, the linear and angular velocity has been obtained with the modeled and simulated kinematics. With it, the acceleration and torque used in each motor have been determined. These data allowed us to feed the calculations of the zero-point moment. The results

obtained indicate that the acceleration value is at the stability limit. Therefore, if they are exceeded, there is a risk of overturning in the "x" direction. Considering the above information, it was defined to do the control taking into account the kinematics of movement of the robot counts an acceleration ramp of three seconds, having as maximum acceleration the maximum value determined in the simulated case (0.045 mt/seg^2).

TABLE 1. Results of the model and simulation

Mode	Wheel angular velocity in the x-axis	Wheel angular acceleratio in the x-axis	Zero moment point		Margin of stability	
			x	y	x	y
Theoretical	5.026 rad/seg	0.6 rad/seg^2	-0.141 mt	-0.044 mt	0.009	0.111
Simulated	5.05 rad/seg	0.601 rad/seg^2	-0.142 mt	-0.0448 mt	0.008	0.11005

Control interface: To operate the robot was developed a user interface in Python using the Tkinter module. The equipment's functions could be considered as telepresence and telemonitoring. Telepresence consists of the robot's remote control using a series of commands activated by the computer keyboard. For the proper handling, the robot was equipped with an audiovisual system that is the voice and image of medical personnel assisting the patient. Telemonitoring consists of the remote measurement of the temperature activated by a command immersed in a virtual button of the user interface. In the upper part of the robot, is incorporated a temperature sensor. It measures the variable at 3 cm from the patient. The current status of the batteries' energy storage is also being checked at all times; allowing us to determine the robot's energy autonomy (Figure 8).

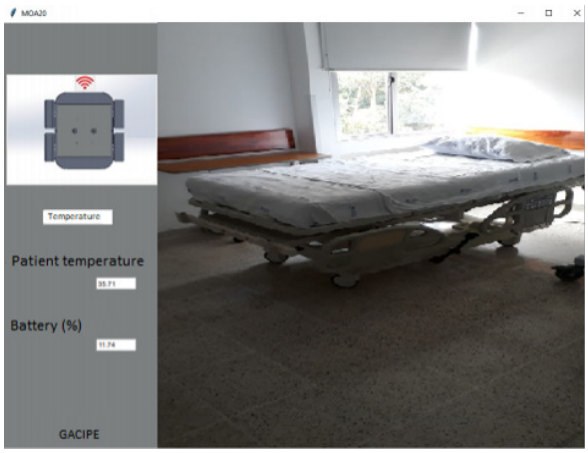

FIGURE 8. Graphical User Interface.

Once the mechanical module, the electronic module, and the graphic interface had been consolidated, the robot's integral operations technical tests were carried out in the laboratory. In the robot operation, the precision of the robot's movements in reduced spaces as verified, the environment monitoring (laser scanner), the measuring of vital signs (temperature), the behavior of the batteries to determine energy autonomy and energy storage management were checked The behavior of the structure was also verified when the cleaning and disinfection process was done. Likewise simulated medical visits to test the link with the WiFi network and the communication between the patient and the health staff were conducted (Figure 9). Finally, the robot's size was determined as follows: 40 cm wide, 40 cm long, and 1.30 cm high.

Verification of the robot's behavior in the clinic: The CUB was in charge of monitoring and handling the robot; during a technical test, this test was developed respecting the internal regulations of the institution. Additionally, the techni-

a) b)

FIGURE 9. Adaptation of the robot to the operating conditions in the clinic. A) Robot RAM. B) User interface.

cal team accompany this tests during the process. It is important to indicate that difficulties were observed with the temperature sensor due to the location, so it was disabled. After that, in the process of appropriation and handling of the robot in the clinic a pilot test. was defined The pilot test is developed, taking into account two stages or moments, which are presented below.

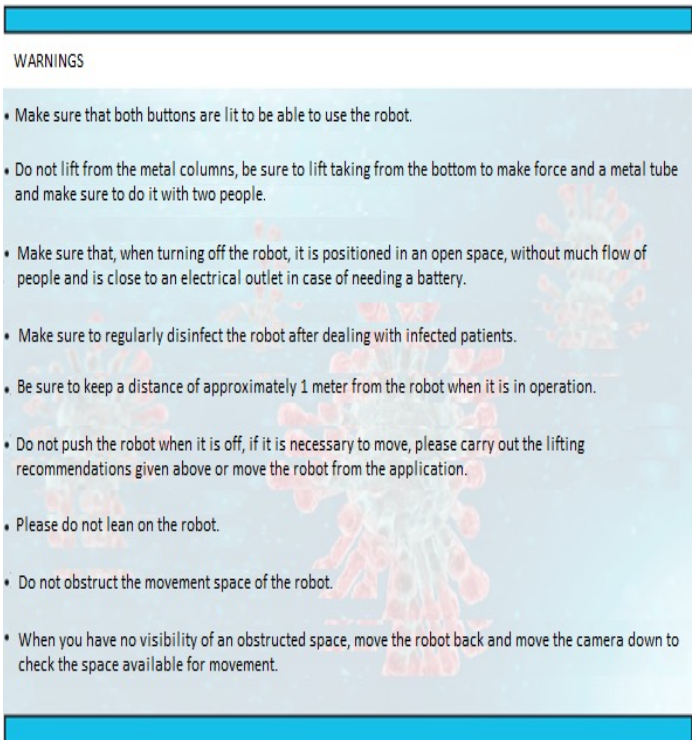

FIGURE 10. Warning instructions.

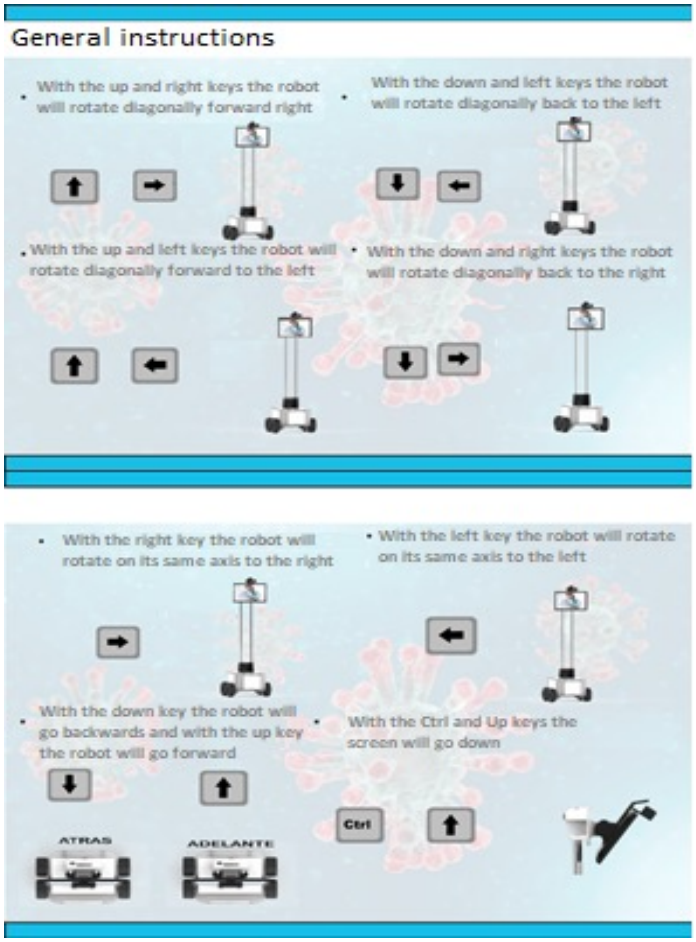

FIGURE 11. General instructions.

Training of health staff: The first stage consisted of the robot's introduction to the health staff, related to the robot's handling. In that process, the user manual and the technical card were introduced. The user manual is a document elaborated with graphic components in which the basic operation of the robot is summarized. The indications presented in the manual are: Warnings, general instructions, interface instructions, start-up, and shut-down process. There are a series of instructions about actions to avoid in the warnings, which might cause damage or trouble in the robot's operation (Figure 10).

The general instructions show the operating instructions for moving the robot using the control system's keyboard (Figure 11).

On the other hand, interface instructions show the special functions incorporated in virtual buttons. These functions are focused on communication and telemonitoring of temperature and energy data (Figure 12).

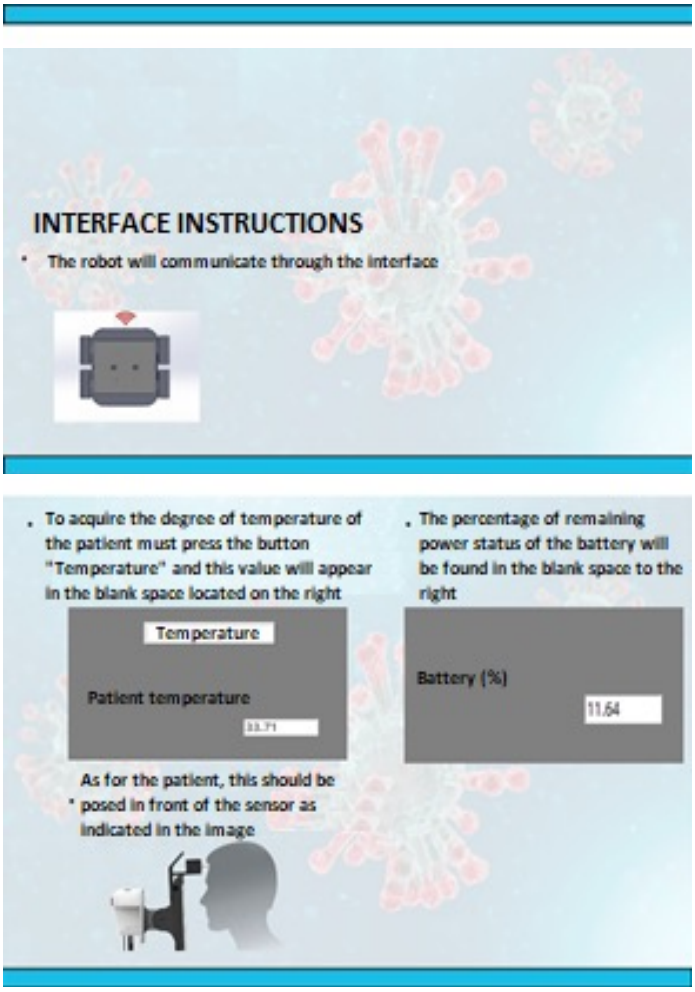

FIGURE 12. **GUI instructions.**

The technical data sheet shows the operational limitations of the robot. Thus, the technical data sheet consists of mechanical, electrical, electronic, and system technical data (see Table 2).

The robot's technical test: The second stage consisted of patient-free tests for robot training and were conducted with the health staff according to the clinic's plan. This allowed the health staff to become familiar with the robot's handling in clinical environments and identify possible obstacles. Also, trials were carried out on video call communication with equipment inside and outside the clinic. Afterward, a consultation was made through a perception survey among the people who participated in the experience, where several of the appreciations were compiled about the robot.

TABLE 2. **Robot technical specifications**

Datasheet GACIPE-MOA20	
Conceived Use	
Robot Medical Assistant	Patient Care Robotics
Dimensions	
HxLxW	130x40x40 cm
Weight	25 kg
Color	
RAL 7001	Grey silver
Loading capacity	
Maximum load on the platform	50kg
Speed and performance	
Autonomy	8 hours
Maximum speed	0.38mt/seg
Turning radius	30 cm
Positioning accuracy	1cm
Power supply	
Battery	Gel 24v 20A
Internal charger	Input 110v 0.28A 60hz Output 12v 8A
Environment	
Ambient temperature range	0 – 50
IP protection class	IP20
Communication	
WiFi	IEEE 802.11.b/g/n/ac 2.4/5 GHz
RF	IEEE 802.15.4 2.4Ghz, 250 Kbps
I/O	HDMI, USB y Ethernet
Sensor	
Laser scanner (Lidar)	360 visual protection around the robot
Interface	
Screen	
Dimensions (HxLxW)	20.79x32.95x2.25 cm
Resolution	1920x1080 Lines
Type	Capacitive Touch Size 13.3”
Camera	
Resolution	720p/30 fps
Sound	
Type	Mono

Cost-benefit relation: The covid-19 pandemic has forced countries to make enormous efforts to try to reduce its spread in the population, especially in the elderly and the health sector community, to such an extent that a study carried out in 73 countries estimated a monthly cost per capita of 8.6 dollars [20], which indicates the large budgets of the countries that have been used to overcome the current crisis. That is why the investment destined in the construction of the robot of 3,500 dollars is beneficial for the health sector since the exposure (of at least 6 people between doctors and nurses per day) to the virus is reduced and therefore the probability of contagion. This means that if the hospital staff rotates every week, and each health worker has at least 1 family member, the number of people with the potential for contagion during a month is 48. Hence the cost-benefit relationship is 0.117, which means that it can achieve the return on investment in at least 9 months, which allows deducing the project's viability.

Analysis of robot results as a technical tool in the hospital: This phase collected all the information. The results obtained were analyzed during the operation of the robot in the hospital environment.

Different actors were tested (medical staff, patients, and technical team), which interacted with the technological tool. The findings found during the pilot test of the robot in the clinic are presented below.

Technical verification of the prototype. The medical assistance simulation sessions developed in the clinic monitored the robot's behavior to determine the technological problems and its functions' performance. Additionally, technical assistance was provided when it was required.

SWOT Matrix. A SWOT matrix as a planning tool is developed to identify the robotic system's potential in the health field. Below is presented the most important aspects found in this process:

- *Weaknesses*

The robot has displacement problems because the wheels tend to slip.

The patient in bed is not displayed through the camera of the robot when they are close. This makes it difficult for the doctor to observe the actual state of the patient.

The robot has blind spots for detecting small objects in its environment.

The control of the robot is complex due to the control instrument's operating limitations (keyboard).

There are problems with the connectivity of the robot to the WiFi system of the clinic. The clinic's WiFi network is not optimal. This problem may reflect an inconvenient dependence on communication quality with the institution's infrastructure.

In a noisy environment, the communication of the robot may experience sound-related problems.

Improve the design of the robot to make friendlier interaction with the patient.

The camera seems to have low quality, and the image is not sharp. Including a higher resolution camera might be beneficial, especially for use in inter-consultation. The camera should also be mobile because this favors the peripheral vision of the robotic system. If these aspects are taken into account, it could optimize the robot displacement and improve the patient's visualization.

To adapt the interface that controls the robot to make the walls, the obstacles, or people's presence more evident.

Driving the robot is difficult with the computer commands. So it is suggested to adopt a device (joystick) to facilitate driving. Another option is using an autonomous displacement system to optimize the time of the medical staff.

- *Threats*

The spaces for the displacement of the robot in the clinic rooms are reduced, and there are irregular objects of difficult detection.

The WiFi bandwidth of the clinics is limited and only used for basic data management.

There is little experience of the medical staff in the handling of this kind of technological tools.

Ramps or stairs can limit the robot's movement in the corridors of the clinics.

Facilitate the proceeding to make the call with the robot and the inclusion of kin helps to not install another application for communication. Using a link to open a video call is susceptible to possible hacking or communication crossing.

- *Strengths*

The sound in both the computer and the robot has good quality when communicating with patients at close range.

The microphone captures well the sound of people in the room because the robot only has to be one meter inside the room to have good communication with the patient.

The robot's remote communication is versatile since both the medical staff and the relatives can communicate with the patient.

The communication between medical staff and patients is good and fluid if there is silence and low traffic on the WiFi network. The people who interacted with the team said they consider it a useful tool for interaction with isolated patients.

- *Opportunities*

The increase in the number of infections among medical staff in clinics due to patients' care with COVID 19.

The existence of the SARS-COV-2 virus in closed and confined places such as clinic rooms.

The insufficient number of medical staff to address the health emergency in the country.

Health staff sees a great projection for future use. They believe it is important to be autonomous in the displacement and have a tray to deliver things.

Strategies: The strategies are labored comparing strengths, opportunities, threats, and weaknesses

Successful approach. With the implementation of remote communication employing the robot between the doctor and the patient, it favors medical safety processes related to COVID 19. Bearing in mind that the attention of a patient in a hospital or clinic requires the health staff.

Reaction approach. The robot's reduced size (40 cm wide, 40 cm long, and 1.30 cm high) and the ability to position itself with turns on its center

facilitate mobility in narrow spaces. It is important to note that hospital and clinic rooms are occupied by multiple objects, furnishings, and equipment.

Adaptive approach. The robot has the function of being used as a tool that virtually brings health staff closer to the patient. To achieve this end, it is imperative to modify the wheels to have more friction with hospital surfaces and to incorporate a camera and screen positioning mechanism to bring the robot as close as possible to the patient.

Survival approach. The robot must be redesigned so that its locomotion module can adapt to sudden changes in environment slopes. There must be another communication option that does not depend on the internet, such as developing local area networks (intranet).

After defining the SWOT matrix and constructing the action strategies, it can deduce that the robotic system has great possibilities of having a positive impact and of becoming a tool of great help for the health staff. To make this impact more effective, it must neutralize the robot's current limitations so that more complex technologies that are less dependent on the hospital infrastructure are incorporated.

Discussion

After doing a brief search for research projects in the year 2020 related to intelligent and robotic systems applied to the health sector and related to the SARS-COV-2 virus pandemic and of the presentation of the work developed with "GACIPE-MOA20" robot, a comparative analysis of the different projects around their potential in the health sector will be carried out. Francesco *et al.* [9] presented an Applicative multiagent architecture like a cognitive model, which can interact with patients and physicians in a changing environment and alert or suggest strategies in a given clinical problem. This architecture is evaluated with the Software Architecture Analysis Method (SAAM), establishing that the architecture is modular and can respond adequately to unplanned changes at run time. Geng *et al.* [10] developing a telerobotic system for remote care in patient rooms in total isolation in hospitals. The research work is focused on the design and development of the robot. The robot has four modules: omnidirectional mobile chassis, double robotic arm, height adjustment mechanisms, and vital signs monitoring devices. The size of the structure of the robot is approximately 60 cm wide. It is currently under observation in clinical trials. Koppu *et al.* [11] raised a disease prediction model tested in simulation with the Cleveland and Starlog datasets related to heart disease. The Wisconsin dataset with breast cancer disease is presented.

Francesco *et al.* [9] and Koppu *et al.* [11] researches are being carried out on information processing architectures with artificial intelligence methods that allow them to make decisions under the medical body's supervision. However, they are currently being studied through simulations in which they have demonstrated their great power. Geng *et al.* [10] proposed to develop a robot equipped with technologies for teleoperation and telepresence with multiple functions such as measurement of vital signs (temperature, heart rate), delivery of medicines, and disinfection of parts or containers of SARS-COV-2 (COVID-19). However, its structural dimensions limit those conventional clinic rooms with multiple objects, equipment, and furnishings. In contrast, the robotic system proposed has already been tested in the clinical environment, performing telepresence and telemonitoring operations in regular rooms and the ICU. Despite some difficulties in the operation, it has received good feedback from the medical staff and patients. Considering that clinics and hospitals are common to find rooms with very reduced spaces for displacement, however, in such

environments, the reduced structure size of the robot (40 cm wide, 40 cm long, and 1.30 cm high) has allowed the robot's normal operation without having problems of blockage or jamming. All the above allows us to consider the prototype a viable technological tool to be used in any clinic or hospital to fulfill functions framed in telecommunication and telemonitoring with patients infected with the SARS-COV-2 virus. In general terms, the Health sector is interested in providing robotic systems with significant attributes which allow them to be competitive in their routine procedures.

CONCLUSIONS

The development of the robot in its different stages of design and implementation with the functions of telepresence and telemonitoring has been consolidated in a short time, leaving the robot at the disposal of the CUB after approximately one month of work.

According to the SWOT matrix analysis and the strategies obtained, it can be possible to say that the robot can become a handy technological tool for health staff as long as the robot's evolution allows them to be independent of the hospital infrastructure. In the aspect of telemonitoring of vital signs, from the beginning, the temperature sensor had some difficulties for the measurement. These were due to the sensor's location that produced defects in the measurement obtained. For the telepresence function, some problems of the robot connectivity with WiFi were found. Also, there were difficulties in the patient's visualization due to the camera's inability to move.

In general terms, there is a positive perception by the medical staff and patients using the robot as a communication and interaction tool in the technical test.

AUTHOR CONTRIBUTIONS

E.M.R.M. was in charge of the coordination of the construction of the robot; S.C.Z., C.A.V.C., L.T.O. and J.S.T.Z. Mechanical development of the robot; J.E.G.M., J.C.L.L., Y.S.J.M. and J.D.A.P. carried out the electronic development of the robot; P.A.P.C. developed the evaluation and technical diagnosis tools of the robot; J.G.B.G. was in charge of the coordination of the prototype test; E.A.T.S. and V.A.A.U. built the evaluation instruments for the prototype test; B.S.J.F. and J.S.P.Z. developed the prototype tests; V.A.A.T. and Y.A.A.P. developed the analysis of the test results. All authors contributed to the writing of the article.

Ethical statement

This project focuses solely on describing a robot's implementation and functionality to remotely establish communication between patient and doctor in a simulated way. This work aims to establish the bases (from the technical point of view) of a robot that, in the future, may have uses in those patients who suffer from infectious diseases such as Covid-19.

REFERENCES

[1] González-Jaramillo V, González-Jaramillo N, Gómez-Restrepo C, et al. Impact of the COVID-19 pandemic on the Colombian population according to mitigation measures. Preliminary data from epidemiological models for the period March 18 to April 18. Rev Sal Pub [Internet]. 2020;22(2):1-6. Available from: https://doi.org/10.15446/rsap.v22n2.85789

[2] Sanchez-Duque JA, Orozco-Hernandez JP, Marin-Medina DS, Arteaga-Livias K, et al. Economy or Health, Constant Dilemma in Times of Pandemic: The case of Coronavirus Disease 2019 (COVID-19). J Pure Appl Microbiol [Internet]. 2020;14(suppl 1):717-720. Available from: https://doi.org/10.22207/JPAM.14.SPL1.07

[3] Acter T, Uddin N, Das J, Akhter A, et al. Evolution of severe acute respiratory syndrome coronavirus 2 (SARS-CoV-2) as coronavirus disease 2019 (COVID-19) pandemic: A global health emergency. Sci Total Environ [Internet]. 2020;730:138996. Available from: https://doi.org/10.1016/j.scitotenv.2020.138996

[4] Climent-Ballester S, Selva-Otaolaurruchi J. Hospital Pharmacy: Comprehensive management of medical devices during SARS-CoV-2. Farm Hosp [Internet]. 2020;44(7):21-23. Available from: https://doi.org/10.7399/fh.11486

[5] Jiang Q, Liu Y, Wei W, Chen A, et al. The Incidence and Epidemic Characteristics of Medical Staff's Skin Injuries Caused by Personal Protective Equipment for Fighting against SARS-CoV-2 Infection. Chinese Gen Pract. 2020;23(9):1083 - 1090.

[6] Rolim Neto ML, Gomes Almeida HG, D'arc Esmeraldo J, et al. When health professionals look death in the eye: the mental health of professionals who deal daily with the 2019 coronavirus outbreak. Psychiatry Res [Internet]. 2020;288:112972. Available from: https://doi.org/10.1016/j.psychres.2020.112972

[7] Jin YH, Huang Q, Wang YY, et al. Perceived infection transmission routes, infection control practices, psychosocial changes, and management of COVID-19 infected healthcare workers in a tertiary acute care hospital in Wuhan: A cross-sectional survey. Military Med Res [Internet]. 2020;7. Available from: https://doi.org/10.1186/s40779-020-00254-8

[8] Győrffy Z, Békási S, Szathmári-Mészáros N, Németh O. Possibilities of telemedicine regarding the COVID-19 pandemic in light of the international and Hungarian experiences and recommendations. Orv Hetilap [Internet]. 2020;161(24):983-992. Hungarian. Available from: https://doi.org/10.1556/650.2020.31873

[9] Lanza F, Seidita V, Chella A. Agents and robots for collaborating and supporting physicians in healthcare scenarios. J Biomed Inform [Internet]. 2020;108:103483. Available from: https://doi.org/10.1016/j.jbi.2020.103483

[10] Yang G, Lv H, Zhang Z, et al. Keep Healthcare Workers Safe: Application of Teleoperated Robot in Isolation Ward for COVID-19 Prevention and Control. Chin J Mech Eng [Internet]. 2020;33:47(2020). Available from: https://doi.org/10.1186/s10033-020-00464-0

[11] Koppu S, Maddikunta PKR, Srivastava G. Deep learning disease prediction model for use with intelligent robots. Comput Electr Eng [Internet]. 2020;87:106765. Available from: https://doi.org/10.1016/j.compeleceng.2020.106765

[12] Farah S, Anderson DG, Langer R. Physical and mechanical properties of PLA, and their functions in widespread applications — A comprehensive review. Adv Drug Deliv Rev [Internet]. 2016;107:367-392. Available from: https://doi.org/10.1016/j.addr.2016.06.012

[13] Zhang YL, Velinsky SA, Feng X. On the Tracking Control of Differentially Steered Wheeled Mobile Robots. J Dyn Syst Meas Control [Internet]. 1997;119(3):455-461. Available from: https://doi.org/10.1115/1.2801278

[14] Muir PF, Neuman CP. Kinematic modeling of wheeled mobile robots. J Robot Syst [Internet]. 1987; 4(2):281-340. Available from: https://doi.org/10.1002/rob.4620040209

[15] Li Y, Dai S, Zheng Y, et al. Modeling and Kinematics Simulation of a Mecanum Wheel Platform in RecurDyn. J Robot [Internet]. 2018; 2018:9373580. Available from: https://doi.org/10.1155/2018/9373580

[16] Zhang S, Gao J, Duan X, et al. Trot pattern generation for quadruped robot based on the ZMP stability margin. In 2013 ICME International Conference on Complex Medical Engineering [Internet]. Beijing: IEEE; 2013:608-613. Available from: https://doi.org/10.1109/ICCME.2013.6548322

[17] Rico Mesa EM, Hernandez-Riveros J-A. Handling the Transition in the Locomotion of an Articulated Quadruped Robot by Adaptive CPG. IAENG Int J Comput Sci. 2020;47(4):792-804.

[18] Sugano S, Huang Q, Kato I. Stability criteria in controlling mobile robotic systems. In Proceedings of 1993 IEEE/RSJ International Conference on Intelligent Robots and Systems (IROS '93) [Internet]. Yokohama: IEEE; 2002: 832-838. Available from: https://doi.org/10.1109/IROS.1993.583186

[19] Kim J, Chung WK. Real-time zero moment point compensation method using null motion for mobile manipulators. Adv Robot [Internet]. 2006;20(5): 581-593. Available from: https://doi.org/10.1163/156855306776985586

[20] Tan-Torres Edejer T, Hanssen O, Mirelman A, et al. Projected health-care resource needs for an effective response to COVID-19 in 73 low-income and middle-income countries: a modelling study. Lancet Glob Health [Internet]. 2020;8(11): e1372 - e1379. Available from: https://doi.org/10.1016/S2214-109X(20)30383-1